Transports and budgets of total inorganic carbon in the subpolar and temperate North Atlantic

Marta Álvarez, Aida F. Ríos, and Fiz F. Pérez
Instituto de Investigaciones Marinas (CSIC), Vigo, Spain

Harry L. Bryden
Southampton Oceanography Centre, Empress Dock, Southampton, UK

Gabriel Rosón
Facultad de Ciencias, Universidade de Vigo, Campus Lagoas-Marcosende, Vigo, Spain

Received 6 February 2002; revised 14 June 2002; accepted 9 September 2002; published 3 January 2003.

[1] Transports of Total Inorganic Carbon (TIC), Total Alkalinity (TA) and Anthropogenic Carbon (C_{ANT}) are calculated across a densely sampled World Ocean Circulation Experiment (WOCE) section at the southern boundary of the subpolar North Atlantic (WOCE A25, 4x cruise). The circulation pattern was approximated using an inverse model constrained with measured mass transports at specific sites, while conserving the mass and salt transports, and forcing the silicate flux to equal the river input north of the section. The mass and chemical fluxes are decomposed into their barotropic, baroclinic and horizontal components. The TA transport is negligible (transport ± maximum estimate of uncertainty, -135 ± 507 kmol s^{-1}), while TIC is transported southwards (-1015 ± 490 kmol s^{-1}) and C_{ANT} northwards (116 ± 125 kmol s^{-1}). Combining our results with those from *Rosón et al.* [2002] across 24.5°N (WOCE A5) we examine the contemporary and preindustrial TIC budgets in the subpolar and temperate North Atlantic based on two different approximations for the budget definitions. Initially, river input, biological production of TIC, along with sedimentation of calcium carbonate are ignored. Then, extended contemporary and preindustrial TIC budgets are discussed including rough estimates of the former processes, mainly based on values from the literature. Our findings point to the North Atlantic Ocean north of 24.5°N as a strong sink for atmospheric CO_2 both today (2932 ± 2057 kmol s^{-1}) and preindustrially (2439 ± 1721 kmol s^{-1}). Only 17% of the contemporary CO_2 air-sea uptake corresponds to C_{ANT}, which is mainly taken up in the temperate North Atlantic (between the 4x and 24.5°N sections). North of 24.5°N the Atlantic Ocean stores C_{ANT} at a rate of 1123 ± 200 kmol s^{-1}. This C_{ANT} is mainly advected into the area in the upper limb of the overturning circulation, while 44% is directly introduced by air-sea uptake. *INDEX TERMS:* 1615 Global Change: Biogeochemical processes (4805); 1635 Global Change: Oceans (4203); 4806 Oceanography: Biological and Chemical: Carbon cycling; 4203 Oceanography: General: Analytical modeling; *KEYWORDS:* North Atlantic, transports and budgets of inorganic carbon, transport and storage of anthropogenic carbon, air-sea CO_2 fluxes

Citation: Álvarez, M., A. F. Ríos, F. F. Pérez, H. L. Bryden, and G. Rosón, Transports and budgets of total inorganic carbon in the subpolar and temperate North Atlantic, *Global Biogeochem. Cycles*, *17*(1), 1002, doi:10.1029/2002GB001881, 2003.

1. Introduction

[2] Before the beginning of the Industrial era the global CO_2 cycle is assumed to have been in steady state [*Sarmiento and Sundquist*, 1992; *Sarmiento et al.*, 2000]. Since then, the burning of fossil fuels and changes in land use have led to a rapid increase of atmospheric CO_2. About half of the anthropogenic CO_2 emissions remain in the atmosphere, the rest is being stored in the ocean and terrestrial biosphere. The carbon inventory changes within an environmental reservoir relative to the inventory that existed during the preindustrial era are defined as "Excess CO_2" or anthropogenic carbon [*Wallace*, 2001]. The current estimate for the oceanic anthropogenic CO_2 sink proposed by the Intergovernmental Panel on Climate Change (IPCC) is 2.0 ± 0.8 Pg C yr^{-1} [*Schimel et al.*, 1996]. This quantity is mainly based on ocean models which are validated with bomb-

0886-6236/03/2002GB001881$12.00

derived ^{14}C [*Orr*, 1993; *Sarmiento et al.*, 1992; *Siegenthaler and Sarmiento*, 1993; *Stocker et al.*, 1994] or calibrated with other transient tracers such as CFCs [*Joos et al.*, 1991a, 1991b; *Siegenthaler and Joos*, 1992]. Atmospheric models with observational $\delta O_2/N$ constraints [*Keeling and Shertz*, 1992; *Keeling et al.*, 1993, 1996] and mass balances based on the distribution of the $^{13}C/^{12}C$ isotope anomaly [*Broecker and Peng*, 1993; *Quay et al.*, 1992; *Tans et al.*, 1993] also support the IPCC estimate.

[3] Direct estimation of the CO_2 anthropogenic uptake by the oceans is no easy task, as the anthropogenic signal in the ocean presents a very low signal-to-noise ratio [*Wallace*, 1995, 2001]. The recent CO_2 climatology by *Takahashi et al.* [1999] estimated the total (anthropogenic and natural signal) CO_2 uptake by the oceans using direct CO_2 measurements and an interpolation method based on lateral 2-D advection-diffusion transport equations and the gas transfer coefficient of *Wanninkhof* [1992], but presented high uncertainties (about 75%) in the final estimates.

[4] Several methodologies have been proposed to extract the anthropogenic CO_2 from oceanic total inorganic carbon measurements. First, the method proposed by *Brewer* [1978] and *Chen and Millero* [1979], the so-called "preformed-CO_2" method or back-calculation technique, corrects measured total inorganic carbon for changes due to organic matter decomposition (ascribed to oxygen changes) and calcium carbonate dissolution (ascribed to alkalinity variations). Based on this approach, an improved method was recently developed by *Gruber et al.* [1996] and further modified by *Pérez et al.* [2002]. In the approximation by *Gruber et al.* [1996] the air-sea CO_2 disequilibrium when a water parcel loses contact with the atmosphere is introduced and accounted for using either water ages from transient tracers or the distribution of biologically-corrected total inorganic carbon in uncontaminated regions. In a succeeding paper *Gruber* [1998] applied the latter method in the Atlantic Ocean, resolving water masses mixing on potential density surfaces.

[5] Ocean carbon transport across transoceanic sections provides valuable information for global carbon cycle research as explained by *Wallace* [2001]. Reliable transports combined with reliable estimates of anthropogenic carbon storage can be used to infer regional air-sea uptake of total, anthropogenic, and preindustrial CO_2. Such independent results are to be compared with the CO_2 uptake provided either by climatologies or models. In this sense, these estimates of the regional distribution of CO_2 uptake will help to validate and/or constrain general circulation models, and therefore aid in predicting the future oceanic CO_2 uptake and consequently global climate change. Hence, there has been an international effort to collect high-quality CO_2 measurements during the World Ocean Circulation Experiment (WOCE) global survey program, as a major component of International Joint Global Ocean Flux Study (JGOFS) (see *Wallace* [2001] for an overview).

[6] The northern North Atlantic Ocean is widely recognised as an area of deep-water formation. Cold deep waters can carry more carbon than warm surface waters suggesting a net uptake and southward transport of CO_2 associated with the North Atlantic branch of the global thermohaline circulation [*Broecker and Peng*, 1992; *Keeling and Peng*, 1995] even during preindustrial times [*Siegenthaler and Sarmiento*, 1993]. According to *Wallace* [1995] the assessment of the CO_2 transport by the North Atlantic meridional circulation received great attention after the controversial paper by *Tans et al.* [1990] as a way to resolve, or at least constrain, the "missing sink" problem [*Schindler*, 1999].

[7] Several studies have investigated the meridional transport of CO_2 across the North Atlantic, from direct estimates [*Brewer et al.*, 1989] or by applying inverse methods to estimate the inorganic carbon flux [*Holfort et al.*, 1998; *Martel and Wunsch*, 1993; *Robbins*, 1994; *Rosón et al.*, 2002; *Stoll et al.*, 1996]. In this work we will present an estimate of the transports of Total Inorganic Carbon (TIC), Total Alkalinity (TA) and Anthropogenic Carbon (C_{ANT}) across a highly-sampled WOCE section at the southern boundary of the Subpolar North Atlantic, along with a description of the main mechanisms responsible for the transports. Additionally, regional budgets for contemporary, preindustrial and anthropogenic carbon will be presented combining our results with those across the 24.5°N (WOCE A5) section in the North Atlantic from *Rosón et al.* [2002].

2. Database

[8] As part of the WOCE program a section from Vigo (north western Iberian Peninsula) to Cape Farewell (south Greenland) (WOCE A25 or 4x section) was occupied in summer 1997 during RRS *Discovery* cruise 230 (Figure 1). Continuous recording of temperature, salinity and pressure was obtained by a Conductivity-Temperature-Depth (CTD) incorporated into a rosette sampler with 24 bottles. Subsamples for salinity, nutrients, oxygen, CFCs and carbon were taken from 10 litre GO water bottles. Here we will briefly describe the methodologies employed for the analysis of each variable with more emphasis on the carbon measurements. A more detailed description about sampling procedures, measurement protocols and data quality control checks is given by *Bacon* [1998].

[9] Salinity samples were analysed on a Guildline 8400A salinometer calibrated with IAPSO Standard Seawater. Nutrients were analysed on board using SOC Chemlab AAII type Auto-Analyser coupled to a Digital-Analysis Microstream data capture and reduction system. Precision for nitrate was evaluated as ± 0.2 μmol kg^{-1}. Oxygen was determined by Winkler potentiometric titration following the indications described in the WOCE Manual of Operations [*Culberson*, 1991]. Oxygen precision was better than 1 μmol kg^{-1}.

[10] Seawater pH was measured using a double wavelength spectrophotometric procedure [*Clayton and Byrne*, 1993]. Absorbance measurements were made by a Beckman DU600 spectrophotometer. Temperature was controlled using a refrigerated circulating temperature bath at 25°C. Total alkalinity was determined by automatic potentiometric titration with HCl to a final pH of 4.44 [*Pérez and Fraga*, 1987]. The electrode was standardised using an NBS buffer of pH 7.413 and checked using an NBS buffer of 4.008. This method has a precision of 0.1% [*Pérez and Fraga*, 1987]. The accuracy of both pH and TA measurements was

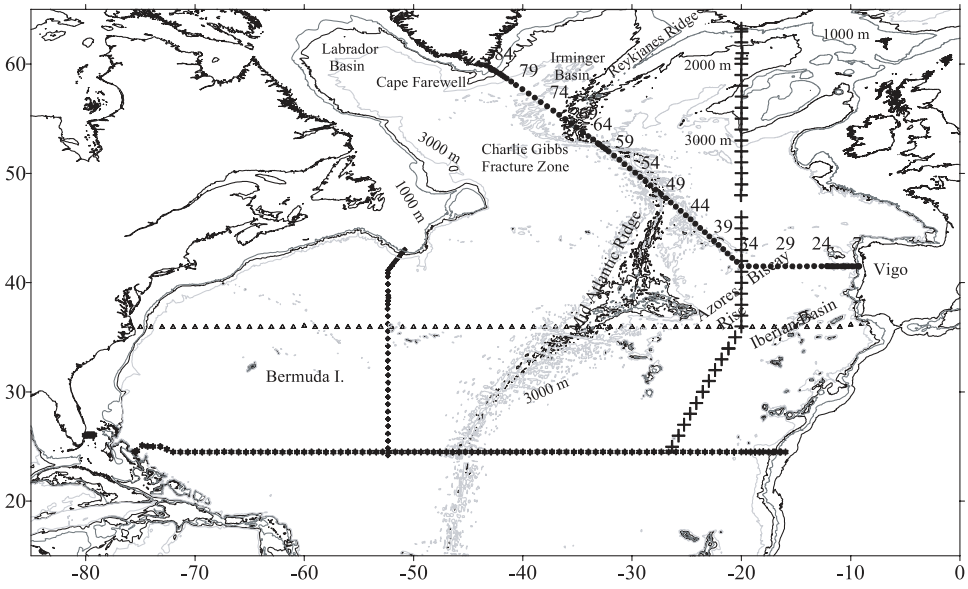

Figure 1. Station locations from the 4x cruise (solid circles), WOCE A20 (diamonds), OacesNAtlII-93 (crosses), 36°N (triangles) and 24.5°N (stars) sections.

controlled by the use of Certified Reference Material supplied by Andrew Dickson from the Scripps Institution of Oceanography, and was calculated to be ±0.002 and ±2 μmol kg^{-1}, respectively.

[11] TIC was estimated from pH and TA data using the thermodynamic equations of the carbonate system [*Dickson*, 1981] and the constants determined by *Mehrbach et al.* [1973] and *Weiss* [1974]. The total error in the TIC estimate taking into account the pH and TA errors was ±3 μmol kg^{-1}, calculated at the average values of pH, TA, salinity and temperature during the cruise.

3. Methods

3.1. Determination of the Transports and Their Components

[12] The net transport of any property across the 4x section can be computed as:

$$T_{Prop} = \int_{Vigo}^{Farewell} \int_{-H}^{0} v \cdot \rho_{S,T,P} \cdot Prop \cdot dx \cdot dz \qquad (1)$$

where T_{Prop} is the transport of any property, calculated by integrating the product of the property concentration (Prop), the velocity orthogonal to the section (v) and the in situ density ($\rho_{S,\,T,\,P}$) from Vigo to Cape Farewell over the entire water column (that is, from the surface, 0, to the bottom depth, −H). The triangular area remaining below the deepest common level at each pair of stations is treated separately: the transport in the bottom triangles is calculated by multiplying the velocity at deepest common level by the bottom triangle area and a weighted average (see the Appendix) of each property in the bottom triangle.

[13] The velocity field is assumed to be geostrophically balanced except for the wind-driven Ekman layer. For calculating the geostrophic velocity with the thermal wind equation, CTD data recorded every 2 dbar for temperature, salinity and pressure are smoothed to 20 dbar intervals for each station. Chemical data obtained at bottle depths are linearly interpolated to 20 dbar intervals, so as to match the physical fields. We make the assumption that the property distributions below the upper 100–200 dbar are uninfluenced by the seasonal cycle and represent long-term distributions in order to obtain a climatological estimate of the transports from a single section. The upper Ekman layer will be treated separately, and will be explained below.

[14] To understand the processes leading to the transports, we have separated the geostrophic fluxes into components as introduced by *Roemmich and Wunsch* [1985], *Bryden et al.* [1991], *Saunders and Thompson* [1993] and *Bryden* [1993]. The geostrophic transport of any property can be broken up into 3 parts, a barotropic term due to the net transport across the section; a baroclinic term due to the horizontally averaged vertical structure; and finally, a horizontal term due to the residual flow after the barotropic and baroclinic components have been subtracted, which is associated with the horizontal variations about the baroclinic profile.

$$\begin{aligned} v &= \langle \overline{v} \rangle + \langle v \rangle(z) + v'(x,z) \\ Prop &= \langle \overline{Prop} \rangle + \langle Prop \rangle(z) + Prop'(x,z) \end{aligned} \qquad (2)$$

The barotropic transport is associated with the net mass transport through the section, whereas the baroclinic and horizontal terms have no net mass flow. The baroclinic and horizontal transports are respectively associated with the meridional overturning circulation and the large-scale gyre circulation including smaller scale eddies. To quantify these components, the orthogonal velocity, v, and each property, Prop, are separated into a section-averaged value ($\langle \overline{v} \rangle$ and $\langle \overline{Prop} \rangle$, respectively), a baroclinic profile of zonally averaged values at each depth ($\langle v \rangle(z)$ and $\langle Prop \rangle(z)$), and

the deviations from zonal averages (anomalies) for each pair of stations and depth ($v'(x,z)$ and $Prop'(x,z)$). Hence, The corresponding transports are calculated as: Barotropic component

$$\rho_{S,T,P} \cdot \langle \bar{v} \rangle \cdot \langle \overline{Prop} \rangle \cdot \int L(z)dz \tag{3a}$$

Baroclinic component

$$\int \rho_{S,T,P} \cdot \langle v \rangle(z) \cdot \langle Prop \rangle(z) \cdot L(z)dz \tag{3b}$$

Horizontal component

$$\int \rho_{S,T,P} \cdot v\prime(x,z) \cdot Prop\prime(x,z) \cdot dz \cdot dx \tag{3c}$$

where L(z) is the width of the section at each depth and $\int L(z)dz$ is the area of the section. The transports are given in kmol s^{-1} (10^3 mol s^{-1}). Throughout we use the convention that positive fluxes refer to northward transports orthogonal to the section.

[15] The Ekman transport of any property is calculated as:

$$T^{Ek}_{Prop} = \int \frac{\tau}{f} \cdot \overline{Prop}_{EK} \cdot dx \tag{4}$$

where τ is the cross-section wind stress component, f the Coriolis parameter and $Prop_{Ek}$ is the mean value of each property in the Ekman layer, taken as 75 dbar. In order to obtain a climatological mean of the circulation, we calculated the seasonal mean Ekman transport, and the corresponding annual mean. Seasonal means for the east and northward wind components were obtained from the Southampton Oceanography Centre (SOC) wind Climatology [*Josey et al.*, 2002]. Multiple linear regressions were calculated for TA and TIC in the upper 200 dbar as a function of temperature, salinity, oxygen and nutrients. Seasonal values for the former variables in the Ekman layer were obtained from the NOAA Atlas 1998. Finally, seasonal values for TA and TIC were interpolated based on the multiple linear regressions and the seasonal values from the NOAA Atlas 1998. Anthropogenic carbon values in the Ekman layer were taken to be those at 130 dbar along the section, as 130 dbar is below the seasonal thermocline. Depths above 130 dbar were homogenized in anthropogenic carbon, so as to avoid biases due to biological activity. Seasonal Ekman wind stress values were coupled with the mean seasonal properties, except for C_{ANT}, and then seasonal transports were averaged to obtain the annual average Ekman property transports.

[16] The determination of the velocity field is thoroughly described by *Álvarez et al.* [2002], here we will just present an overview of the process. Initially the circulation pattern is approximated in order to reproduce the closest-to-reality estimate of the velocity field. This is our "initial guess" which is finally introduced into an inverse model with additional constraints so as to obtain the "best estimate" of the circulation. Careful attention was paid in the definition of the "initial guess" as the inverse model results will depend on it [*Rintoul and Wunsch*, 1991]. The geostrophic velocity was initially calculated referenced for a fixed Level of No Motion (LNM) equal to 3200 dbar [*Saunders*, 1982]. Then, the LNM was changed to σ_2 = 36.94 kg m^{-3} everywhere except for the Iberian Abyssal Plain. The resulting mass imbalance was uniformly distributed across the section to make the net mass flux be zero. Based on direct observations and reliable estimates of the mass transport at specific areas crossed by the section, we adjusted the mass flux at three locations: the Iberian Abyssal Plain (IAP), the Charlie-Gibbs Fracture Zone (CGFZ) and the western boundary region within 110 km of Greenland, in the East Greenland Current (EGC). Specifically, the mass transport was adjusted to zero below about 2000 dbar in the IAP, to −2.4 Sv (1 Sv = 10^6 m^3 s^{-1}) southwards in the CGFZ for waters with $\sigma_\theta > 27.8$ kg m^{-3} [*Saunders*, 1994] and to −25 Sv southwards for the whole water column in the EGC [*Bacon*, 1997]. We assume that the net flow between Greenland and Europe is small (0 ± 1 Sv) [see *Álvarez et al.*, 2002], which is the same as assuming the North Atlantic Ocean north of the 4x section to be a closed basin. Therefore, salt conservation instead of mass conservation is required, since the freshwater balance does not affect salt. With the "initial guess" circulation pattern a high silicate flux (−105 kmol s^{-1}) was obtained. Consequently, an inverse model was used to set the silicate transport to equal the riverine input of silicate north of the section (26 kmol s^{-1}, estimated from the recent review of the silica cycle by *Tréguer et al.* [1995]), along with conserving salt and minimising the total net mass flux. Minor reference level corrections were calculated with the inverse model; after their application over the "initial guess" circulation the "best estimate" circulation is obtained. In the Appendix the applied methodology to estimate the main sources of uncertainty affecting the fluxes is described, giving a final value for the maximum error on each transport estimate.

3.2. Estimation of C_{ANT}

[17] In this work we use the approximation for calculating C_{ANT} suggested by *Pérez et al.* [2002] based on improvements to the back-calculation technique originally proposed by *Brewer* [1978] and *Chen and Millero* [1979] and further modified by *Gruber et al.* [1996]. In their paper, *Pérez et al.* [2002] showed evidence for the inaccurate estimate of preformed alkalinity (TA^0) and TIC in equilibrium with the preindustrial atmospheric CO_2 ($TIC^{eq\pi}$) proposed by *Gruber et al.* [1996]. A new parameterization for TA^0 was suggested as a function of the Apparent Oxygen Utilization (AOU) and the inorganic to organic carbon decomposition ratio. The influence of water vapor partial pressure in calculating the preindustrial level of CO_2 atmospheric partial pressure and the use of an appropriate set of dissociation constants, concretely those from *Mehrbach et al.* [1973], were also evaluated in the estimate of $TIC^{eq\pi}$. Applying these improvements to the *Gruber et al.* [1996] methodology, *Pérez et al.* [2002] questioned the existence of the high disequilibrium term (TICdis) proposed by *Gruber et al.* [1996] because evidence from direct CO_2 data taken on formation areas suggests that ΔTICdis is negligible.

[18] Thus, C_{ANT} is estimated here as:

$$C_{ANT} = TIC - AOU/R_C - 1/2\left(TA - TA^0 + AOU/R_N\right) - TIC^{eq\pi} \quad (5)$$

where AOU is calculated using the oxygen saturation equation from Benson and Krause [*U.N. Educational, Scientific, and Cultural Organization*, 1986]. We used R_C = 1.45 ± 0.17 and R_N = 10.6 ± 0.7 [*Anderson and Sarmiento*, 1994]. TA^0 is calculated as given by *Pérez et al.* [2002]; $TIC^{eq\pi}$ is estimated from the time-independent TA^0 and the preindustrial atmospheric CO_2 level [*Neftel et al.*, 1994].

[19] The possible sources of uncertainty in the C_{ANT} calculation mainly arise from the uncertainty in the stoichiometric ratios, the estimate of TA^0 and $TIC^{eq\pi}$, the sampling and measurement errors and finally, the disregarded air-sea oxygen and carbon disequilibrium when the water is formed. Using a Gaussian error propagation analysis for C_{ANT} as given by *Gruber et al.* [1996] or *Sabine et al.* [1999], the random errors associated with the anthropogenic CO_2 calculation are given by:

$$\begin{aligned}\{\sigma_{CANT}\}^2 = {} & \{\sigma_{TIC}\}^2 + \{\sigma_{TICeq\pi}\}^2 + \{-(O_2 - O_{2sat})\cdot\sigma_{RC}\}^2 \\ & + \{(-1/R_C - 0.5\cdot 1/R_N)\cdot\sigma_{O2}\}^2 \\ & + \{(1/R_C + 0.5\cdot 1/R_N)\cdot\sigma_{O2sat}\}^2 + \{0.5\cdot\sigma_{TA}\}^2 \\ & + \left\{\left(-\frac{\delta TIC^{eq\pi}}{\delta TA^0} + 0.5\right)\cdot\sigma_{TA0}\right\}^2 \\ & + \{-0.5\cdot(O_2 - O_{2sat})\cdot\sigma_{RN}\}^2 \\ & + \{-(O_2 - O_{2sat})\cdot\sigma_{RC}\}^2 + \{\sigma_{TICdis}\}^2 \end{aligned} \quad (6)$$

where σ_{TIC} = 3 μmol kg^{-1}, σ_{TA} = 2 μmol kg^{-1}, σ_{O2} = 1 μmol kg^{-1} (analytical errors), σ_{O2sat} = 4 μmol kg^{-1}, $\frac{\delta TIC^{eq\pi}}{\delta TA}$ = 0.852, $\sigma_{TICeq\pi}$ = 4 μmol kg^{-1} (previous estimates from *Gruber et al.* [1996]), σ_{TA0}= 3 μmol kg^{-1}, σ_{TICdis}= 4 μmol kg^{-1} (errors given in *Pérez et al.*, 2002), σ_{RC} = 0.092 and σ_{RN} = 0.0081 [from *Anderson and Sarmiento*, 1994]. The terms involving R_C and R_N were evaluated separately because random errors cannot be distinguished from systematic errors, both depend on the magnitude of AOU. A negligible error is ascribed to the R_N term [*Gruber et al.*, 1996]. Given the range of our AOU values the error ascribed to the R_C term has a mean value of 4 μmol kg^{-1}. Thus, the estimated error of C_{ANT} is 7.4 μmol kg^{-1}. Similar to the values proposed by *Gruber et al.* [1996], *Körtzinger et al.* [1998] or *Sabine et al.* [1999]. However, the average C_{ANT} content for waters deeper than 4000 dbar is 5.2 ± 4 μmol kg^{-1}, indicating that the previous error estimate must express the maximum random variability since the averaging effect acting on independent errors decreases the random errors considerably.

4. Distributions, Transports, and Mechanisms

[20] As an overview, in this section we will first comment on the vertical distribution of the chemical properties along the 4x section. Next, a brief description is given of the three components into which they are decomposed, barotropic, baroclinic and horizontal, in order to understand the mechanisms controlling the final transport values.

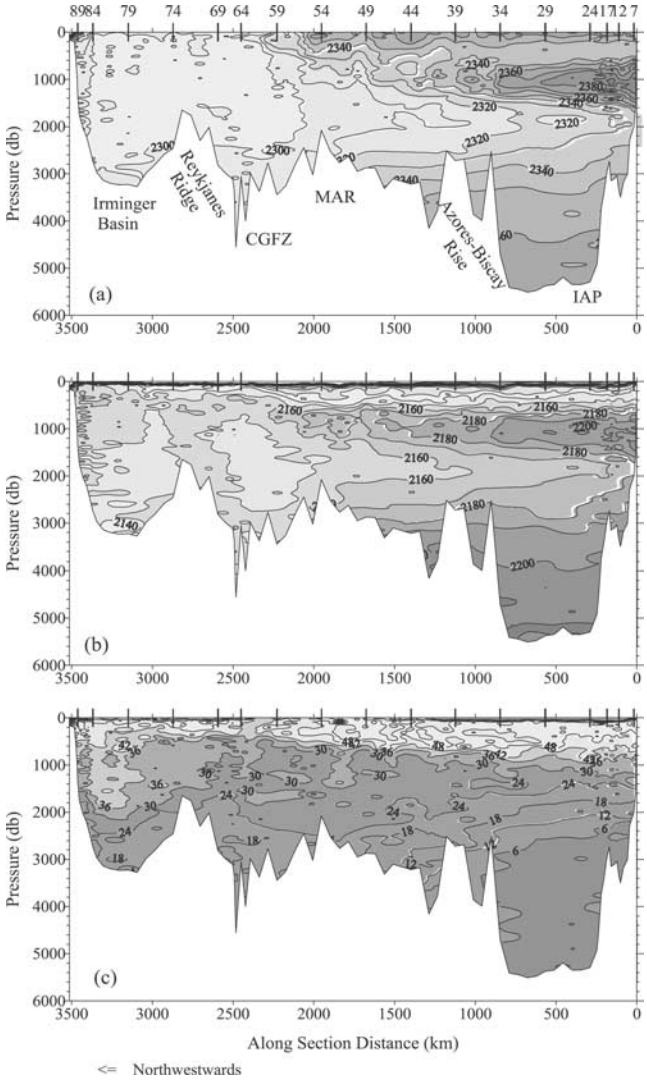

Figure 2. Vertical distribution along the 4x section of (a) total alkalinity (TA), (b) total inorganic carbon (TIC) and (c) anthropogenic carbon (C_{ANT}), all properties in μmol kg^{-1}. The upper axis shows station positions. Geographic areas are highlighted: MAR stands for Mid-Atlantic Ridge, CGFZ for Charlie-Gibbs Fracture Zone and IAP for Iberian Abyssal Plain. See color version of this figure at back of this issue

4.1. Chemical Distributions and Decomposition

[21] A thorough description of the water masses chemical characterization along the 4x section using a mixing model is given by M. Álvarez et al. (Mixing analysis in the North Atlantic subpolar gyre, submitted to *Deep Sea Research, Part I*, 2002) (hereinafter referred to as Álvarez et al., submitted manuscript, 2002). Briefly, the 4x section crosses a variety of water masses. In the upper 500 dbar, Eastern North Atlantic Central Water dominates east of the North Atlantic Current (NAC). The NAC is clearly discerned as a steep TA gradient in the upper 1000 dbar between stations 59 and 64, over the CGFZ (Figure 2a). In the eastern basin, at about 1000 dbar the Mediterranean Water (MW) signal is evidenced by its TA and TIC maximum (Figures 2a and 2b).

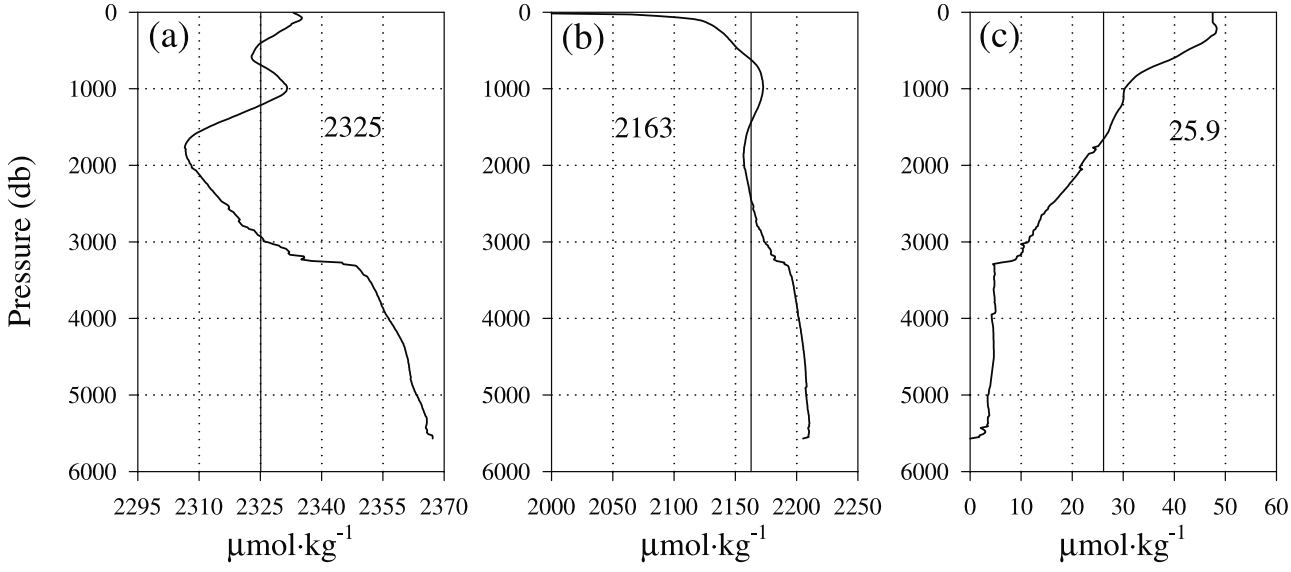

Figure 3. Zonal average profile of (a) total alkalinity (TA), (b) total inorganic carbon (TIC) and (c) anthropogenic carbon (C_{ANT}), along with the corresponding section mean values, all properties in μmol kg^{-1}. The baroclinic profile is the deviation from the mean as a function of depth.

Labrador Sea Water (LSW) is situated below MW with lower TA and TIC content, it extends from the Labrador basin into the Irminger basin, accounting for the homogeneous TA and TIC content between 1000 and 2500 dbar. Another branch of the LSW crosses the Mid-Atlantic Ridge (MAR) entering the eastern basin, and is detected as a highly ventilated water mass. The 4x section crosses the path of the two Nordic overflows, the Denmark Strait Overflow Water (DSOW) and the Iceland-Scotland Overflow Water (ISOW) (Álvarez et al., submitted manuscript, 2002). The DSOW influence is mainly detected at the bottom along the western side of the Irminger basin, it is characterized by a temperature minimum with TA and TIC values lower than the LSW (Figures 2a and 2b). The ISOW influence is detected as a salinity maximum mainly at the bottom of the CGFZ western flank, with relatively high TA and TIC values with respect to the overlying LSW.

[22] The C_{ANT} isolines have a general upward tilt towards the east, as more recently formed waters with a higher C_{ANT} content are found towards the western end of the section. In this sense, at the LSW level, about 1500 dbar, a clear eastward decrease of C_{ANT} is revealed due to mixing with older water masses but also due to the influence from older vintages of LSW. According to *Cunningham and Haine* [1995] 20 years are needed for LSW to reach the eastern North Atlantic from the Labrador basin. DSOW and ISOW influenced water below 3000 dbar in the Irminger basin and CGFZ present C_{ANT} concentrations of 21 ± 2 μmol kg^{-1} and 18 ± 2 μmol kg^{-1}, respectively, revealing its recent formation.

[23] As described in the Methods section, the properties are decomposed into three components (Figures 3 and 4). The section mean values are ascribed to the barotropic component: 2325, 2163 and 26 μmol kg^{-1} for TA, TIC and C_{ANT}, respectively. These values multiplied by the barotropic mass transport yield the corresponding barotropic transport of the property across the section (Table 1). The area weighted vertical profile of each property is shown in Figure 3. Vertical deviations of this profile from the section mean correspond to the baroclinic component of the properties, which combined with the corresponding baroclinic mass transport yield the transport ascribed to the overturning circulation.

[24] The area weighted vertical profile of TA (Figure 3a) presents a maximum at 1000 dbar ascribed to MW influence, and a minimum at about 1700 dbar related to LSW. TA increases downward with a steep gradient between 3000 and 3500 dbar, below this depth the profile mainly reflects the characteristics of the IAP deep waters as the rest of the 4x section is shallower.

[25] The TIC profile (Figure 3b) also reflects the MW and LSW influence at 1000 and 1500 dbar, with a relative maximum and minimum, respectively. The 4x section crosses an area of recently formed water masses. Thus, is not surprising to find significant C_{ANT} signal down to 3200 dbar (Figure 3c), in the same way as *Körtzinger et al.* [1998] found in the North Atlantic western basin at about 46°N. In contrast, at 24.5°N, *Rosón et al.* [2002] found a significant anthropogenic CO_2 content only in the upper 1500 dbar as a mean. Below 3200 dbar (Figure 3c) a steep gradient separates the upper "contaminated" waters from IAP deep waters with a negligible C_{ANT}.

[26] The horizontal component of each property is calculated as the anomaly of the distribution of the property from its area weighted vertical profile. The anomalies show the horizontal or along-section differences in the chemical distributions. For example, at 1000 dbar the TA anomalies (Figure 4a) reveal the contrasting TA content between MW (high) and LSW (low) on the eastern and western ends of the section, respectively. TIC anomalies (Figure 4b) also

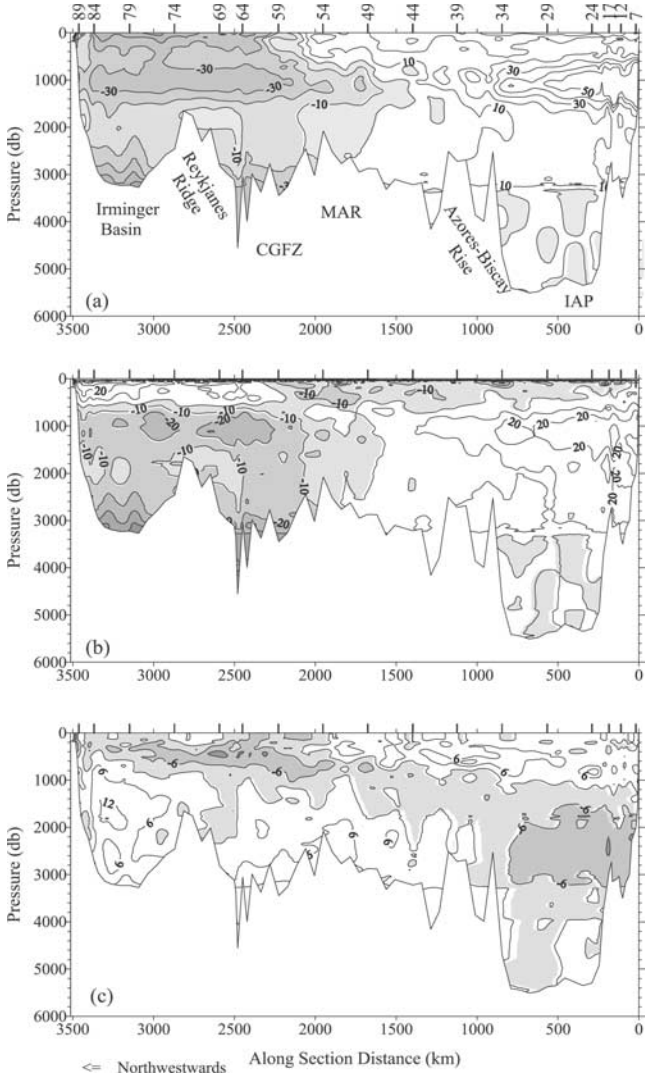

Figure 4. Vertical distribution along the 4x section of the (a) total alkalinity (TA), (b) total inorganic carbon (TIC) and (c) anthropogenic carbon (C_{ANT}) anomalies, all properties expressed in μmol kg^{-1}. The upper axis shows station positions. Geographic areas are highlighted: MAR stands for Mid-Atlantic Ridge, CGFZ for Charlie-Gibbs Fracture Zone and IAP for Iberian Abyssal Plain.

show the contrasting TIC concentration at 1000 dbar. As well, at 3000 dbar deep waters on the western end have a lower TIC content than those in the IAP. The C_{ANT} anomalies (Figure 4c) confirm the previous comments about the C_{ANT} vertical distribution along the 4x section (Figure 2c), with higher C_{ANT} values towards the west especially at the LSW and overflow.

4.2. Transports and Their Mechanisms

[27] The magnitudes of the decomposed and final mass, salt and chemical transports and corresponding maximum errors (See Appendix) are given in Table 1. The mass and salt transports across the 4x section are commented upon by *Álvarez et al.* [2002]. As an overview, the final mass transport is −0.4 ± 1.5 Sv southwestward (hereafter SW) with a negligible salt transport, therefore, it corresponds to a net precipitation plus runoff over evaporation over the basin north of our section.

[28] The North Atlantic Ocean north of the 4x section exports TIC southwestward at a rate of −1081 kmol s^{-1}. Yet, this value is biased as the section was sampled in summer. If the upper 210 dbar are homogenized with the TIC at 210 dbar to simulate deep winter mixing, the TIC transport is reduced to −949 kmol s^{-1}, thus the approximated annual mean for the TIC transport would be −1015 ± 490 kmol s^{-1}. However, to maintain the consistency of our exposition, we will concentrate on the results from the real TIC data taken during the cruise. C_{ANT} is imported at 116 ± 125 kmol s^{-1} from the southwest, whereas the TA transport, within the given range of uncertainty, is not significantly different from zero, −135 ± 507 kmol s^{-1}.

[29] The baroclinic or overturning circulation drives a northeastward (hereinafter NE) flow of 14.8 Sv in the upper 1000 dbar (Figure 5a), mainly ascribed to the NAC system, which is compensated by a SW flow of −16.5 Sv at intermediate levels. Below 3200 dbar there is a NE flow of 1.7 Sv. The horizontally integrated mass transport accumulated from zero at the east (Figure 5e) shows the two main horizontal currents across the section, the NAC and the EGC, situated from 1700 to 2500 km and within 110 km of Greenland (3390–3500 km), and transporting 28.4 Sv and −25.4 Sv, respectively [see *Álvarez et al.*, 2002].

[30] The total barotropic transport across the section derives from the combination of the barotropic component, the transport in the bottom triangles and that at the Ekman layer (Table 1). Due to this net SW mass transport (−0.4 Sv), −872, −770 and −31 kmol s^{-1} of TA, TIC and C_{ANT} are flowing SW, respectively. The SW total barotropic TA transport is practically compensated by the NE baroclinic and horizontal components, in accordance with the salt transport, as TA and salinity have a strong relationship. Regarding TIC, the overturning circulation drives a total SW flow of −315 kmol s^{-1} (Table 1), with the main flow in the upper 1000 dbar (−378 kmol s^{-1}) (Figure 5c). In this

Table 1. "Best Estimate" Transports Across the 4x Section and Corresponding Maximum Errors[a]

	Barotropic	Bottom Transport	Ekman	Total Barotropic	Baroclinic	Horizontal	Final	Error
Mass - Sv	5.26	−4.28	−1.38	−0.40	0.00	0.00	−0.40	1.48
Salt - Mkg s^{-1}	191.3	−155.8	−49.9	−14.4	5.8	7.8	−0.8	6.7
TA - kmol s^{-1}	12671	−10252	−3291	−872	284	453	−135	507
TIC - kmol s^{-1}	11788	−9586	−2972	−770	−315	4	−1081	490
C_{ANT} - kmol s^{-1}	141	−105	−67	−31	352	−205	116	125

[a]Units are Sv (10^6 m^3 s^{-1}), Mkg s^{-1} (10^6 kg s^{-1}) and kmol s^{-1} (10^3 mol s^{-1}).

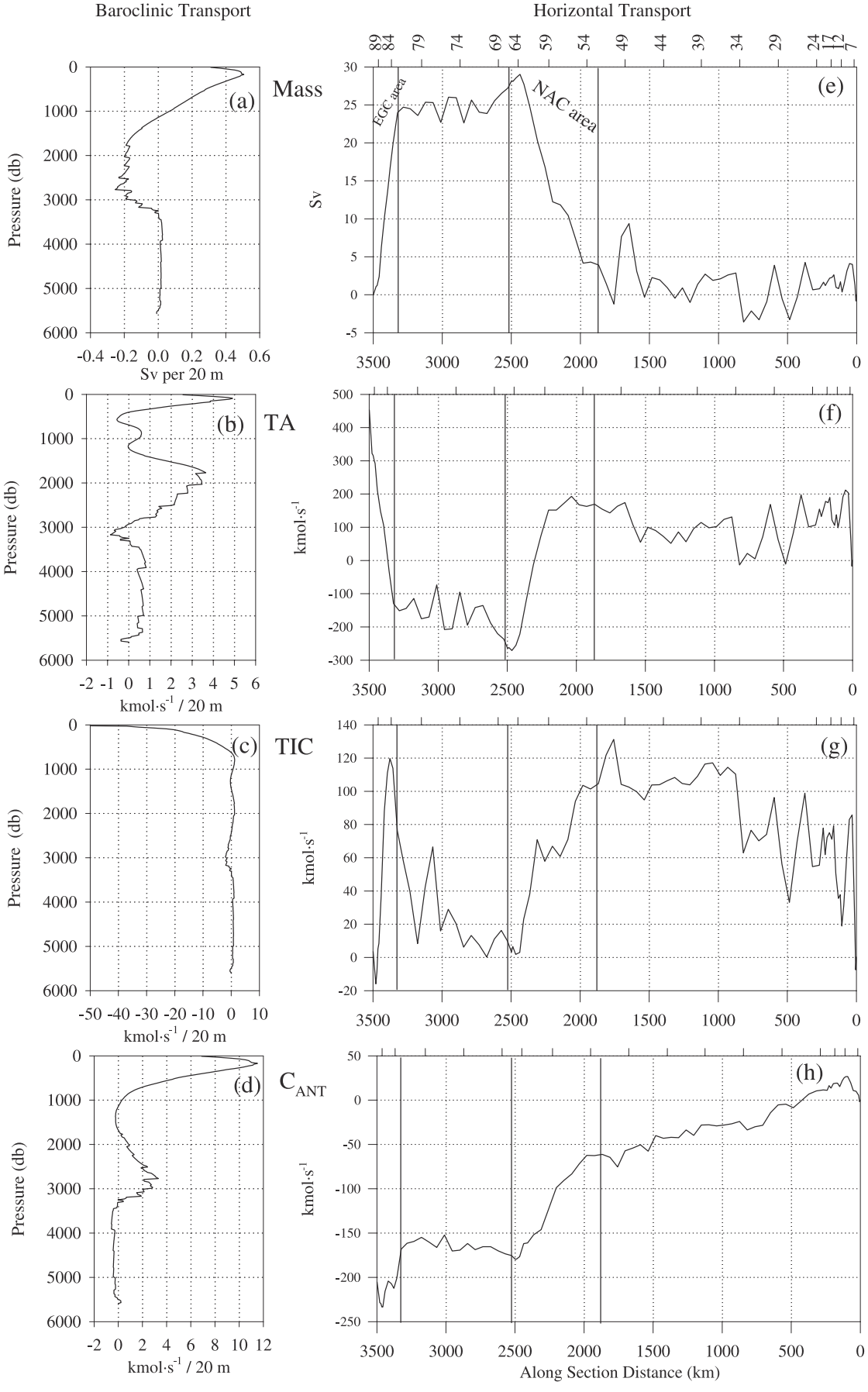
Baroclinic Transport
Horizontal Transport
Mass
TA
TIC
C_ANT
(a)
(b)
(c)
(d)
(e)
(f)
(g)
(h)
Pressure (db)
Sv per 20 m
kmol·s-1 / 20 m
Sv
kmol·s-1
EGC area
NAC area
Along Section Distance (km)

layer TIC-poor waters (Figure 3b) flow NE (Figure 5a), effectively removing or exporting TIC from the North Atlantic Ocean north of the 4x section. Whereas, below 1000 dbar the total baroclinic TIC flow is 63 kmol s^{-1} NE. The overturning TIC transport in the Subpolar gyre can be understood as a vertical belt in which TIC-poor upper waters flow NE and return SW at deeper levels TIC enriched. The enrichment mechanism is related to the solubility pump: while flowing NE the upper water cools [*Álvarez et al.*, 2002], gaining TIC because CO_2 solubility increases with decreasing temperature. In contrast the horizontal circulation presents a small contribution to the final TIC transport (Table 1). TIC-enriched waters are horizontally transported east of the MAR (about 2000 km from Vigo), this horizontal northeastward TIC transport is balanced by the northeastward flow of TIC-poor waters in the NAC (Figure 5g). The TIC horizontal transport up to the MAR amounts to 104 kmol s^{-1}, in the NAC the TIC transport is −91 kmol s^{-1} and in the EGC −107 kmol s^{-1}.

[31] The total barotropic C_{ANT} transport is −31 kmol s^{-1}, the horizontal cell also contributes with a SW transport of −205 kmol s^{-1} (Table 1). Thus, the main mechanism responsible for the NE C_{ANT} total transport across the 4x section is the overturning circulation, with 352 kmol s^{-1}. The baroclinic C_{ANT} transport profile (Figure 5d) reveals a two-lobe structure, in which C_{ANT}-rich (relative to the section mean) waters flow NE in the upper 1700 dbar and deeper C_{ANT}-poor (relative to the section mean) waters return SW (Figure 3c and 5a). Thus, the upper layer directly transports C_{ANT} NE and the lower one leaves C_{ANT} north of the section, being equivalent to a NE transport of C_{ANT} across the 4x section.

[32] The C_{ANT} horizontal transport (Figure 5h) shows that the NAC and the transport in the Irminger basin (1700–2500 km and west of 3000 km, respectively) mainly drive the SW C_{ANT} horizontal transport, contributing −108 and −31 kmol s^{-1}, respectively. In the NAC system the C_{ANT} anomalies are mainly negative compared to the section mean profile (Figure 4c), but the mass transport anomalies are positive, resulting in the NAC horizontally removing C_{ANT} from the North Atlantic Subpolar gyre. In the Irminger basin the C_{ANT} anomalies are mainly positive and the water flows SW, thus the horizontal export of C_{ANT}. In this case, the waters flowing NE east of the MAR transport less C_{ANT} than those returning SW at the same depth level on the western side of the MAR, ending up with a final SW C_{ANT} horizontal transport of −205 kmol s^{-1}.

[33] Summing up, the net mass transport across the 4x section reflects the freshwater balance north of the section. This barotropic net flux drives a SW transport of chemical properties. This transport, in the case of TA, is compensated by the overturning and horizontal cells, ending up with practically negligible TA flux across the section. In contrast, TIC is transported SW mainly due to the barotropic mass flow but with a smaller contribution from the overturning cell. This cell acts in the upper 1000 dbar as a removal pump of carbon north of the section, transporting TIC poor waters NE. Surprisingly, the horizontal transport of TIC is practically balanced, the NE transport east of the MAR is mainly compensated in the NAC and EGC. In the case of C_{ANT}, a final NE flow of 116 kmol s^{-1} is calculated. The overturning cell carries C_{ANT} NE, transported in the upper 1000 dbar, and as an indirect consequence leaving C_{ANT}-rich waters north of the section at intermediate levels. The horizontal cell drives a SW C_{ANT} transport concentrated in the NAC and the Irminger Basin current systems.

[34] If the total Bering Strait flow of −0.8 Sv [*Roach et al.*, 1995] is added barotropically across the 4x section flowing at the section mean values for TA, TIC and C_{ANT}, there would be additional southward transports of −1927, −1792 and −22 kmol s^{-1} across the 4x section and the final transports would be −2062, −2873 and 94 kmol s^{-1}, respectively.

5. Inorganic Carbon Budget for the North Atlantic

[35] In this section we will examine the inorganic carbon budget for the Arctic-Subpolar (from the Bering Strait to the 4x section) and the Temperate (between the 4x and the 24.5°N section) regions, see Figure 1. This analysis is performed combining our results for the inorganic carbon transport with those from *Rosón et al.* [2002] across the 24.5°N zonal section.

[36] As thoroughly discussed by *Holfort et al.* [1998] careful attention must be paid when combining fluxes in order to avoid comparing unlike transport estimates. *Rosón et al.* [2002] and our study followed similar approaches to define the mass transport, taking into account the net freshwater balance north of the sections. *Rosón et al.* [2002], in contrast to this study, accounted for the Bering Strait contribution to the mass and chemical transports. In this sense, for the sake of consistency and considering that we will examine regional convergences or divergences, the Bering Strait contribution will be ignored in the following budgets.

[37] The temporal evolution of contemporary TIC (CONT) includes the temporal variation of its anthropogenic (ANT) and preindustrial (π) components, which should equal the inputs (I) minus the outputs (O) of TIC within the region. Thus,

$$\left(\frac{\Delta TIC}{\Delta t}\right)_{CONT} = \left(\frac{\Delta TIC}{\Delta t}\right)_{\pi} + \left(\frac{\Delta TIC}{\Delta t}\right)_{ANT} = I - O. \qquad (7a)$$

We assume that the preindustrial TIC cycle was operating in steady state [*Sarmiento and Sundquist*, 1992; *Sarmiento et*

Figure 5. (opposite) Baroclinic (a-d) and horizontal (e-h) components of the mass, total alkalinity (TA), total inorganic carbon (TIC) and anthropogenic carbon (C_{ANT}) transports across the 4x section. The horizontal transport is accumulated from zero at Vigo (right end). The upper axis in Figures 5e–5h shows station positions. The vertically integrated baroclinic mass transport down to 1000 dbar is 14.8 Sv, −16.5 Sv from 1100 to 3200 dbar and below 3200 dbar 1.7 Sv. (1 Sv = 10^6 m^3 s^{-1} and 1 kmol s^{-1} = 10^3 mol s^{-1}). The NAC (North Atlantic Current) and EGC (East Greenland Current) areas are delimited by vertical lines.

al., 1992; *Sarmiento et al.*, 2000]. Thus, the temporal evolution of preindustrial TIC equals zero and the temporal evolution of contemporary TIC is in fact the accumulation or storage of anthropogenic carbon within the region. The storage stands for the CO_2 dissolved in the ocean as a result of the total or partial equilibration of surface ocean waters with the increasing atmospheric CO_2 content. Additionally, this anthropogenic CO_2 increase is treated as a perturbation from the preindustrial steady state and, being independent of its biological and geological aspects, does not affect the natural carbon cycle [*Sarmiento et al.*, 1992]. Moreover, we will disregard the riverine input of TIC, production of organic carbon, its burial into the sediments and the dissolution or burial of calcium carbonate in the sediments, as they are supposed to compensate by one another [*Holfort et al.*, 1998; *Rosón et al.*, 2002; *Sarmiento et al.*, 1995; *Stoll et al.*, 1996]. Therefore equation 7a for contemporary TIC can be initially expressed as:

$$\text{Storage} = F_{\text{air-sea CONT}} + T_{\text{S CONT}} + T_{\text{N CONT}} \tag{7b}$$

where the storage is always positive, $F_{\text{air-sea}}$ is the air-sea CO_2 flux in the region (positive into the region), T_S and T_N respectively refer to the net transport of carbon across the southern and northern boundaries of the area (positive into the region). The contemporary inorganic carbon budgets performed in this work are referred to 1995 since the 4x and 24.5°N sections were done in 1997 and 1992, respectively.

[38] As we assumed that the anthropogenic component of the budget is independent and uncorrelated with the preindustrial and contemporary components equation 7a can be expressed just for anthropogenic carbon:

$$\text{Storage} = F_{\text{air-sea ANT}} + T_{\text{S ANT}} + T_{\text{N ANT}} \tag{7c}$$

where all the terms have been defined before, but now refer just to the anthropogenic component of the fluxes across the boundaries of the region.

[39] Subtraction of the C_{ANT} transport from the contemporary TIC transport gives an estimate of the preindustrial TIC (TIC^{π}) transport assuming that the patterns of circulation have remained constant. Therefore, we can estimate budgets for TIC^{π} using the following equation:

$$0 = F_{\text{air-sea }\pi} + T_{\text{S}\pi} + T_{\text{N}\pi}. \tag{7d}$$

5.1. C_{ANT} Storage Estimation

[40] As previously stated, the storage term indicates the magnitude of the anthropogenic inorganic carbon accumulated in the ocean, *i.e.*, the temporal increase of the C_{ANT} inventory. Thus it can be mathematically defined as:

$$\text{Storage} = \frac{d\int C_{ANTz}dz}{dt} \tag{8}$$

where t is time and $\int C_{ANTz}\,dz$ is the water column inventory of C_{ANT}. Its temporal evolution can be only derived from TIC data covering a wide temporal range. The scarcity of quality TIC measurements over a long-enough period of time prevents a reliable direct estimate of this rate. However, it can be derived indirectly. The Mean Penetration Depth (MPD) of any tracer was defined by *Broecker et al.* [1979] as:

$$\text{MPD} = \frac{\int C_{ANTz}dz}{C_{ANTml}} \tag{9}$$

where C_{ANTz} and C_{ANTml} are the C_{ANT} concentrations at any depth (z) and at the mixed layer (mL), respectively. The MPD reflects the circulation pattern: in areas of deep-water formation or active convection MPD is deeper, whilst in areas with high surface stratification the MPD is shallower. The C_{ANT} inventory can be derived from equation 9 as:

$$\frac{\int C_{Antz}dz}{dt} = \text{MPD} \cdot C_{ANTml} \tag{10}$$

whose temporal derivative is:

$$\frac{d\int C_{ANTz}dz}{dt} = \frac{d\text{MPD}}{dt} \cdot C_{ANTml} + \text{MPD} \cdot \frac{dC_{ANTml}}{dt}. \tag{11a}$$

[41] Assuming that C_{ANT} is a conservative tracer (not affected by biology) increasing exponentially at the sea surface with an e-folding time of t years, it would reach its "transient steady state" after 3 × t years [*Gammon et al.*, 1982]. Given that anthropogenic carbon has been increasing since at least 1800 it should by now have achieved the transient state [*Holfort et al.*, 1998]. Thus the shape and scale depth, i.e., the MPD, of the C_{ANT} vertical profile would be constant with time [*Broecker and Peng*, 1982; *Gammon et al.*, 1982]. Therefore, the storage term can be approximated as:

$$\text{Storage} = \frac{d\int C_{ANTz}dz}{dt} = \text{MPD} \cdot \frac{dC_{ANTml}}{dt}. \tag{11b}$$

[42] Therefore, the C_{ANT} storage can be directly calculated from the MPD derived from current TIC observations and the temporal change of C_{ANT} in the mixed layer. Correspondingly, the temporal increase of C_{ANT} in the mixed layer is approximated assuming a fully CO_2 equilibrated mixed layer keeping pace with the CO_2 atmospheric increase (from 0.7 to 0.9 μmol kg^{-1} yr^{-1} depending on the initial temperature, salinity and alkalinity conditions). This approximation for the storage term was used and corroborated by *Holfort et al.* [1998] in the South Atlantic ocean between 10°S and 30°S using WOCE data. *Hoppema et al.* [1998] found an anthropogenic TIC increase of 1.1 μmol kg^{-1} yr^{-1} in the Weddell Sea Deep Water in agreement with the theoretical increase of atmospheric CO_2 in the Southern Ocean. The anthropogenic CO_2 uptake rates calculated by *Wanninkhof et al.* [1999] from an isopycnal analysis in the North Atlantic Ocean agree with those expected for an upper thermocline in equilibrium with the atmospheric CO_2 (from 0.85 to 1.18 μmol kg^{-1} yr^{-1}). A higher value has been reported for the TIC increase in the mixed layer of the Bermuda Atlantic Time-series Study (BATS) site, 1.7 μmol kg^{-1} yr^{-1} [*Bates et al.*, 1996].

[43] There is further evidence confirming the aforementioned approximation. The C_{ANT} MPD along the 41.5°N

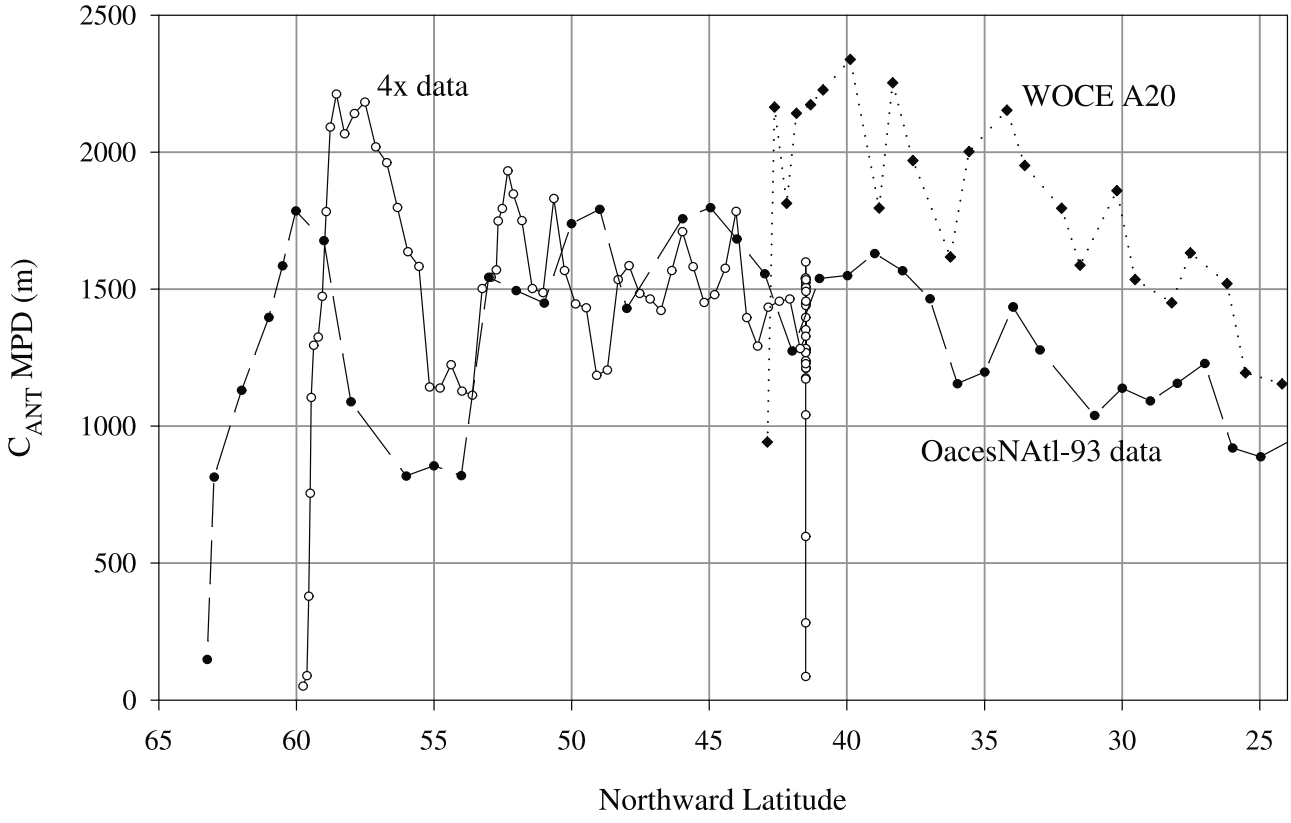

Figure 6. Mean penetration depth (MPD in meters) of anthropogenic carbon against latitude along the OacesNAtl-93 (solid circles), WOCE A20 (diamonds) and 4x (open circles) sections. MPD is calculated as in equation (9), from 150 m to the bottom.

zonal section in the Eastern North Atlantic comprised within the 4x section (Figure 1) is 1360 ± 149 m (Figure 6). This MPD multiplied by the theoretical C_{ANT} rate of increase in the mixed layer of the area, 0.92 μmol kg^{-1} yr^{-1} [*Ríos et al.*, 2001] gives an increasing C_{ANT} inventory of 1.28 ± 0.14 mol m^{-2} yr^{-1}. Given the uncertainties, our fluxes are in agreement with the value of 0.95 mol m^{-2} yr^{-1} directly calculated by *Ríos et al.* [2001] analysing a temporal data set covering from 1977 to 1997 in the Eastern North Atlantic.

[44] Our study areas, the Arctic-Subpolar and the Temperate regions present completely different circulation patterns [*Schmitz*, 1996]. Additionally, the lower limb of the conveyor belt, the Deep Western Boundary Current (DWBC), flows in the western basin of the Temperate region. The DWBC transports relatively recently formed waters at depth, thus the higher content of anthropogenic carbon in the western than in the eastern basins of the North Atlantic [*Gruber*, 1998; *Körtzinger et al.*, 1998]. In the following paragraphs we will explain how we assessed the C_{ANT} storage within these former regions.

[45] The Arctic Ocean and the Greenland Sea C_{ANT} storage are taken as 68.7 and 6.34 kmol s^{-1} from *Anderson et al.* [1998a] and *Anderson et al.* [2000], respectively. The Greenland Sea inventory is linearly extrapolated to the total GIN (Greenland, Iceland and Norwegian) seas area, to be 67.4 kmol s^{-1}.

[46] From 60°N to 24.5°N the North Atlantic Ocean is subdivided in 5° width latitude bands, seven in total. Within each band we distinguished between the western and the eastern basin where a mean and standard deviation MPD are calculated for anthropogenic carbon. In order to complete our picture of the C_{ANT} storage in the North Atlantic, two more data sets were included in this analysis: the OacesNAtlII-93 (www.aoml.noaa.gov/ocd/oaces) section along 20°W from 24°N to 60°N and the WOCE A20 data (www.cdiac.esd.ornl.gov) along 52°W from 24°N to 42°N. C_{ANT} along these two lines was calculated as given by *Pérez et al.* [2002]. The corresponding MPD was calculated with equation 9 disregarding the upper 150 dbar in order to avoid biases in the C_{ANT} content due to biological activity.

[47] The latitudinal variation of the MPD along these three lines is shown in Figure 6. There is a notable increase of the MPD towards the north until about 40°N in both the western (A20 line) and eastern (Oaces line) basins. However, the MPDs in the western basin are approximately 68% deeper than in the eastern basin. From 40° to 50°N the MPDs slightly increase in the eastern basin. In the Irminger Sea (4x data from 55° to 60°N, western basin), the MPD reaches 2300 m as the 4x line crosses the deepest areas along the main overflow pathways (Figure 1).

[48] The former MPDs are multiplied by a mean C_{ANT} rate of increase in the mixed layer of 0.85 μmol kg^{-1} yr^{-1} in

Table 2a. Mean Penetration Depth of Anthropogenic Carbon, C_{ANT} Rates of Increase (mol m^{-2} yr^{-1}), Areas by Latitude Band and Basin[a]

Latitude Band	Basin	MPD, m	C_{ANT} Rate of Increase, mol m^{-2} yr^{-1}	Area, 10^{12} m^2	Storage Rate, kmol s^{-1}
24.5°–30°N	East	1070 ± 137	0.93 ± 0.12	2.4	72 ± 9
	West	1466 ± 166	1.28 ± 0.14	2.4	99 ± 11
30°–35°N	East	1277 ± 168	1.11 ± 0.15	1.4	49 ± 7
	West	1871 ± 240	1.63 ± 0.21	2.1	109 ± 14
35°–40°N	East	1473 ± 187	1.28 ± 0.16	1.2	50 ± 6
	West	2029 ± 262	1.77 ± 0.23	2.3	128 ± 17
40°–45°N	East	1410 ± 168	1.23 ± 0.15	1.0	40 ± 5
	West	2104 ± 166	1.83 ± 0.14	1.9	110 ± 9
45°–50°N	East	1520 ± 168	1.32 ± 0.15	0.8	35 ± 4
	West	1921 ± 152	1.67 ± 0.13	1.6	82 ± 7
50°–55°N	East	1462 ± 321	1.27 ± 0.28	1.3	53 ± 12
	West	1921 ± 152	1.67 ± 0.13	1.3	70 ± 6
55°–60°N	East	1302 ± 432	1.13 ± 0.38	1.2	42 ± 14
	West	1739 ± 381	1.51 ± 0.33	1.0	48 ± 11

[a]The mean C_{ANT} rate of increase in the mixed layer used was 0.85 μmol kg^{-1} yr^{-1}. The storage rates for the Arctic Ocean (asterisk) and the GIN (Greenland-Iceland-Norwegian) seas (plus sign) are also shown. The final storage rates for the Arctic-Subpolar (north of the 4x section) and Temperate (between the 4x and the 24.5°N sections) regions are shown at the bottom. Mean Penetration Depth: MPD in meters, estimated according to equation (9); Anthropogenic Carbon: C_{ANT}, mean ± standard deviation.

order to obtain the C_{ANT} storage rate (in mol m^{-2} yr^{-1}) (Table 2). The storage rates when integrated over the oceanic surface area for each latitude band and basin yield the corresponding C_{ANT} storage (Table 2). Finally, the storage rates are proportionally partitioned into the initial areas defined by the 4x and 24.5°N hydrographic sections (Table 2). So that the final C_{ANT} storage within the Arctic-Subpolar region is 288 ± 100 kmol s^{-1}, and within the Temperate region is 835 ± 100 kmol s^{-1}.

5.2. Initial Budgets

[49] Figure 7 shows a schematic summary of the regional budgets for contemporary TIC, C_{ANT} and TIC^{π}. The air-sea exchange is estimated by the difference between the storage and the flux divergence across the lateral boundaries according to equation 7. As mentioned previously, the North Atlantic Ocean is treated as a closed basin, so the Bering Strait contribution is ignored in these estimates. The contemporary TIC transport across the 4x section indicates a divergence of inorganic carbon in the Arctic-Subpolar region balanced by an air to sea flux of 1303 ± 459 kmol s^{-1} (6.9 ± 2.4 mmol m^{-2} d^{-1}, inferred flux ± maximum error as described in the Appendix) and the storage of C_{ANT}, 288 ± 100 kmol s^{-1} (1.5 ± 1 mmol m^{-2} d^{-1}). Likewise, in the Temperate region the inorganic carbon divergence is balanced by high air to sea flux (2250 ± 532 kmol s^{-1}, 9.5 ± 2.2 mmol m^{-2} d^{-1}) and C_{ANT} storage (835 ± 100 kmol s^{-1}, 3.5 ± 0.4 mmol m^{-2} d^{-1}) (Figure 7a). Looking separately at the C_{ANT} fluxes, the northward flow of C_{ANT} across both sections combined with the storage rates leads to an uptake of C_{ANT} across the air-sea interface of 172 ± 152 kmol s^{-1} (0.9 ± 0.8 mmol m^{-2} d^{-1}) in the northern area and a larger influx of 321 ± 258 kmol s^{-1} (1.4 ± 1.1 mmol m^2 d^{-1}) in the Temperate region (Figure 7b). Regarding the preindustrial budget, the TIC^{π} divergence in the Arctic-Subpolar and Temperate regions is compensated by the corresponding influxes of CO_2 from the atmosphere (Figure 7c), again larger in the Temperate zone than in the northern area.

[50] Our contemporary air-sea fluxes for TIC (1303 and 2250 kmol s^{-1} for the northern and southern regions, respectively) can be compared with independent estimates derived from surface partial pressure CO_2 (pCO_2) data by *Takahashi et al.* [1999] (See Table 3). These authors report a net annual air-sea flux referred to 1995 of 1322 and 847 kmol s^{-1} for the 80°N-4x and Temperate regions, respectively. The uncertainty of these estimates could be as high as 75% [*Holfort et al.*, 1998; *Takahashi et al.*, 1995, 1999]. The lack of pCO_2 data for the Arctic precluded them from obtaining a reliable estimate of the CO_2 air-sea flux in this area. *Anderson et al.* [1998b] estimated an air-sea uptake of 64 ± 26 kmol s^{-1} in the Arctic in agreement with the results of *Lundberg and Haugan* [1996]. Thus the total air-sea flux in the Arctic-Subpolar region would be 1386 kmol s^{-1}. Our air-sea fluxes are thus in reasonable agreement with the independent estimates based on the work of *Takahashi et al.* [1999] and *Anderson et al.* [1998b] in the northern area. However, the discrepancy is obvious in the Temperate region, our air-sea flux seems too high. Can we explain this discrepancy considering the budget for organic carbon as well as the riverine contribution of TIC as proposed in recent review chapters *Doney et al.*, 2000; *Wallace et al.*, 2001] or papers dealing with TIC transports [*Holfort et al.*, 1998; *Stoll et al.*, 1996]?

5.3. Extended Budgets

[51] In this section we will assess the importance of riverine input of TIC, the carbonate sedimentation and the biological production/consumption in balancing regional

Table 2b. Final Storage Rates (kmol^{s-1}) for the Arctic-Subpolar (North of the 4x Section) and Temperate (Between the Rx and the 24.5°N Sections) Regions

Arctic-Subpolar	Temperate
67.4+	
68.7*	
152 ± 50	
288 ± 100	835 ± 100

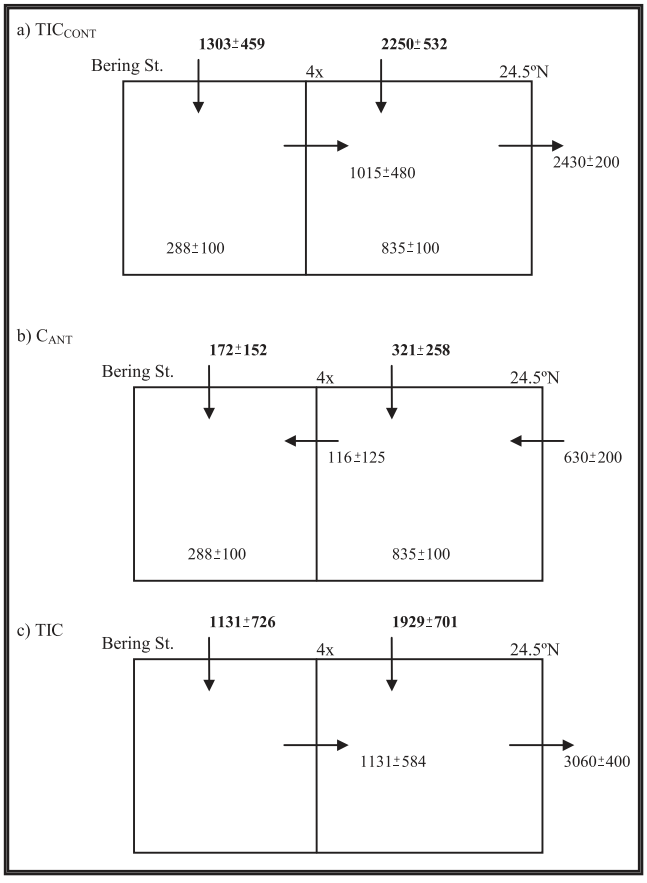

Figure 7. Schematic summary of the regional initial inorganic carbon budgets in the North Atlantic. The Arctic-Subpolar region comprises the area within the Bering Strait and the 4x section and the Temperate region the area within the 4x and the 24.5°N sections. Transports (plain numbers) and air-sea fluxes (bold numbers) are indicated by arrows, the anthropogenic storage term with plain positive numbers. All the terms in kmol s^{-1} (1 Gt C yr^{-1} = 2642 kmol s^{-1}). Budgets for (a) contemporary total inorganic carbon (TIC_{CONT}), (b) anthropogenic carbon (C_{ANT}) and (c) preindustrial TIC (TIC^{π}). The preindustrial TIC budget is the difference between the contemporary and the anthropogenic TIC budgets. The Bering Strait contribution in the transports across sections has been ignored for consistency.

budgets for contemporary (CONT) and preindustrial (π) TIC, previously defined with equations 7b and 7d, respectively. These budgets will be our extended budgets and correspondingly defined as,

$$\text{Storage} = F_{\text{air-sea CONT}} + T_{\text{S CONT}} + T_{\text{N CONT}} + NP_{\text{TIC}} + R_{\text{TIC}} - S_{\text{CaCO3}} \quad (12a)$$

$$0 = F_{\text{air-sea p}} + T_{\text{S}\pi} + T_{\text{N}\pi} + NP_{\text{TIC}} + R_{\text{TIC}} - S_{\text{CaCO3}} \quad (12b)$$

where NP_{TIC} stands for the net production of TIC due to biological activity, that is, the TIC produced throughout the whole water column by the respiration of autotrophes and heterotrophes minus the TIC consumed in the photosynthesis; R_{TIC} stands for the riverine contribution and S_{CaCO3} for the sedimentation of calcium carbonate.

5.3.1. Riverine Input

[52] The recent paper by *Aumont et al.* [2001] evaluates the impact of river carbon discharge on the interhemispheric carbon transport. According to these authors, the river carbon loop resolves the discrepancy between model-based and data-based estimates of the ocean interhemispheric transport of carbon.

[53] Most of the total carbon discharge (85%) is located in the northern hemisphere, specifically 56% of the total carbon discharge is released in the Arctic and North Atlantic Ocean with a higher inorganic to organic carbon ratio. The river input of TIC into the Arctic was estimated by *Anderson et al.* [1998b] to be 90 kmol s^{-1}. The total riverine input is about 1085 ± 77 kmol s^{-1} [*Berner and Berner*, 1987; *Drever et al.*, 1988; *Meybeck*, 1987] and the total river runoff into the ocean is 1.195 Sv, 0.085 Sv into the area from the southern limit of the Arctic and the 4x section, and 0.10 Sv between the 4x and the 24.5°N sections [*Baumgartner and Reichel*, 1975]. Assuming a homogenous riverine TIC input, 77 and 91 kmol s^{-1} are introduced in the Subpolar and the Temperate regions, respectively.

5.3.2. Carbonate Sedimentation

[54] The carbonate production and accumulation in the oceans was estimated by *Milliman* [1993]. Since most of the Atlantic basin lies above the calcite lysocline the carbonate accumulation in this ocean accounts for more than 40% of the global deep-sea total carbonate accumulation. *Milliman* [1993] gives a direct estimate of the carbonate precipitation in the Arctic ocean of 14 kmol s^{-1}. A rough assessment of the carbonate precipitation in the other study regions can

Table 3. Summary of the Air to Sea (±Maximum Error Incurred in the Estimation) Fluxes in kmol s^{-1} Obtained in This Work From the Inorganic Carbon Initial and Extended Budgets and Those Taken From Other Works[a]

	Contemporary			Preindustrial	
	This Work		Other Works	This Work	
	Initial	Extended		Initial	Extended
Arctic-Subpolar	1303 ± 459	864 ± 488	1386 $_{(1,2)}$[b]	1131 ± 726	692 ± 600
Temperate	2250 ± 532	2068 ± 1569	847 $_{(2)}$[b]	1929 ± 701	1747 ± 1121

[a]Other works: 1, *Anderson et al.* [1998b]; 2, *Takahashi et al.* [1999].
[b]Uncertainties of about 75%.

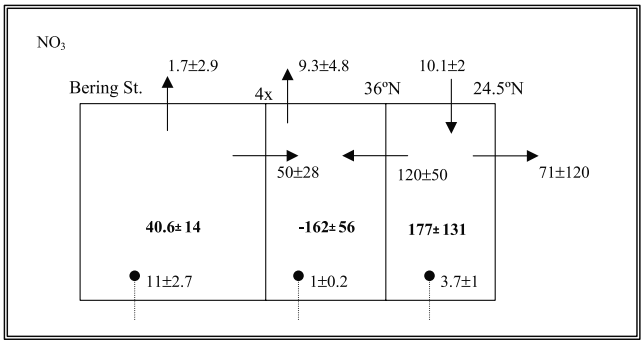

Figure 8. Schematic summary of the regional North Atlantic nitrate budget. The regions are comprised within the Bering Strait and the 4x section, the 4x and the 36°N sections and the 36°N and 24.5°N sections. Units are in kmol s^{-1}. Transports across sections and air-sea fluxes are indicated by arrows, other sources by point-ended arrows and changes due to net production as plain bold numbers, a minus (plus) stands for consumption (production) of the property within each defined box. The Bering Strait contribution in the transports across sections has been ignored for consistency.

be estimated from his Table 3. South of the Arctic and north of the 4x section the accumulation amounts to 11 kmol s^{-1}, and between the 4x and the 24.5°N sections about 19 kmol s^{-1}.

5.3.3. Biological Production/Consumption of TIC

[55] The regional production/consumption of biological TIC can be indirectly derived from regional nitrate budgets assuming steady state for this nutrient within the temporal scale of the regional flushing time. This biological production of TIC corresponds to the whole water column balance between the production of TIC due to the respiration of autotrophes and heterotrophes and the photosynthetic TIC consumption.

5.3.3.1. Nitrate Budgets

[56] Nitrate budgets north of 36°N were presented and discussed by *Álvarez et al.* [2002]. The nitrate budget for the Arctic-Subpolar region points to a production of nitrate in this area of about 40.6 ± 14 kmol s^{-1}, whereas within the 4x and the 36°N sections the budget suggests a nitrate consumption of −162 ± 56 kmol s^{-1} [*Álvarez et al.*, 2002] (Figure 8). We will complete the former analysis with a tentative nitrate budget for the area between the 36°N and 24.5°N zonal sections.

[57] In the same way as for the region north of 36°N given by *Álvarez et al.* [2002], the nitrate (NO_3) budget between 36°N and 24.5°N is assumed to be in steady state for the regional overturning time:

$$\frac{\Delta NO_3}{\Delta t} = I - O + NP_{NO_3} = 0 \qquad (13)$$

The inputs (I) minus the outputs (O) of nitrate must be balanced by the net production of nitrate due to biological activity (NP_{NO3}, stands for the whole water column production of nitrate due to the respiration of autotrophes and heterotrophes minus the consumption by phytoplankton). The nitrate transports across 36°N and 24.5°N are taken from *Rintoul and Wunsch* [1991] and *Lavín* [1999], respectively, as 120 ± 35 and −71 ± 120 kmol s^{-1} (no contribution from the Bering Strait). The atmospheric deposition of nitrate in the open ocean of this region according to *Prospero et al.* [1996] is about 2 kmol s^{-1}, with a negligible deposition over the coastal ocean of about 0.24 kmol s^{-1}. *Howarth et al.* [1996] estimated the total nitrogen input due to river runoff into the coastal areas between 36°N and 24.5°N to be 1.4 kmol s^{-1}. Assuming a 26% contribution of nitrate [*Wollast*, 1993] yields a riverine nitrate input of 0.4 kmol s^{-1}. The estimated denitrification in the region is about 3.1 kmol s^{-1} according to *Nixon et al.* [1996]. The nitrate flow out of the Mediterranean Sea amounts to 3.3 kmol s^{-1} [*Sarmiento et al.*, 1988]. The atmospheric fixation of nitrogen is estimated as 11 kmol s^{-1} for the region [*Lipschultz and Owens*, 1996]. Thus, applying equation 13:

$$NP_{NO_3} = O - I = 120 + 71 - 2 - 0.24 - 0.4 + 3.1 - 3.3 - 11 = 177\,\text{kmol}\cdot s^{-1} \qquad (14)$$

we conclude that there is a net production of nitrate in the 36–24.5°N region of 177 ± 131 kmol s^{-1}, mostly a consequence of boundary fluxes (Figure 8). This net production mainly results from the decomposition of organic matter imported from the north as concluded by *Álvarez et al.* [2002], *Rintoul and Wunsch* [1991] and *Walsh et al.* [1992]. These findings need confirmation from actual estimates of organic matter transports but are supported by indirect evidence of a high nitrate remineralization [*Sarmiento et al.*, 1990] and oxygen consumption [*Jenkins and Goldman*, 1985] within the region. In particular, *Sarmiento et al.* [1990] obtained a nitrate remineralization rate equal to 0.93 ± 0.11 mol m^{-2} yr^{-1} within the thermocline layer (100 to 750 m) of this region based on radon measurements. The difference between the former value and the total whole column remineralization rate obtained here (0.55 ± 0.4 mol m^{-2} yr^{-1} for an area of about 10.2×10^{12} m^2) yields a net import of nitrate into the upper 100 m of about 0.38 mol m^{-2} yr^{-1}, which can be ascribed to new production. Despite the great uncertainties involved, this number is consistent with earlier estimates of 0.6 ± 0.2 mol m^{-2} yr^{-1} by *Jenkins* [1988], the particle flux at 100 m of 0.33 mol m^{-2} yr^{-1} by *Altabet* [1989] and the estimate of 0.42 ± 0.24 mol m^{-2} yr^{-1} by *Sarmiento et al.* [1990].

5.3.3.2. Biological Production of TIC

[58] The nitrate remineralization in the Arctic-Subpolar region translates into a TIC production of 297 ± 102 kmol s^{-1} using the C:N ratio by *Anderson and Sarmiento* [1994] of 7.31. Between the 4x and 36°N sections, TIC is consumed at −1184 ± 500 kmol s^{-1} but in the oligotrophic 36°N–24.5°N region TIC is produced at 1294 ± 958 kmol s^{-1} (see Figure 8).

[59] If we assume that the cycle for organic carbon is in steady state within the time scale of the regional flushing time (this is just for its labile fraction), the biologically-mediated production (consumption) of TIC translates into a consumption (production) of organic carbon, which in turn

should compensate for the outputs minus the inputs of organic carbon within the region. Therefore, the net consumption/production of organic carbon should be balanced by the organic carbon introduced (atmospheric deposition, river input, transport into the region across the lateral boundaries) within the region minus that exported out of it (sedimentation, transport out across the boundaries of the region). It is far beyond the scope of this work to evaluate those terms. We are aware that estimates of organic carbon transport across transoceanic sections in the North Atlantic will eventually be available (Álvarez-Salgado and Hansell, personal communication).

5.3.4. Extended Contemporary and Preindustrial TIC Budgets

[60] Including coarse estimates of river input, calcite sedimentation and biological processes changes the contemporary TIC budget (from Figures 7a to 9a, see Table 3 for a summary). The CO_2 air-sea flux within the Arctic-Subpolar region is considerably reduced from 1303 ± 459 to 864 ± 488 kmol s^{-1}, mainly as a consequence of the net heterotrophic behaviour of the area. In contrast, the CO_2 air-sea flux in the Temperate area is only slightly changed, from 2250 ± 532 to 2068 ± 1569 kmol s^{-1} because the biological pump in the Temperate area only introduces 110 kmol s^{-1} of TIC, as the net autotrophy within the 4x and 36°N region is practically balanced by the net heterotrophy in the 36°N–24.5°N area.

[61] In comparison with the CO_2 flux estimates of 1386 kmol s^{-1} based on the work by *Takahashi et al.* [1999] and *Anderson et al.* [1998b], the new CO_2 air-sea flux in the northernmost region (864 ± 488 kmol s^{-1}) is significantly lower. In the 4x-24.5°N region our CO_2 flux (2068 ± 1569 kmol s^{-1}) is higher than that calculated by *Takahashi et al.* [1999] (847 kmol s^{-1}) (Table 3).

[62] *Watson et al.* [1995] have estimated the maximum air-sea CO_2 flux driven by the heat loss in the North Atlantic Ocean to be 0.75 Gt C yr^{-1} or 1982 kmol s^{-1} for each PW. The northward heat transport across the 4x and 24.5°N section is 0.65 ± 0.1 PW and 1.47 ± 0.4 PW according to *Álvarez et al.* [2002] and *Lavín et al.* [1998], respectively. In consequence, in the Arctic-Subpolar region the thermally-driven influx of CO_2 would be 1288 ± 595 kmol s^{-1} and in the Temperate region about 1625 ± 595 kmol s^{-1}.

[63] In the northernmost region the air-sea CO_2 flux is mostly driven by the heat loss to the atmosphere (1288 ± 595 kmol s^{-1}) minus the biological CO_2 production (297 ± 102 kmol s^{-1}) yields 991 ± 697 kmol s^{-1}, in fairly good agreement with the final net CO_2 air-sea flux of 864 ± 488 kmol s^{-1}. Within the Temperate region most of the air-sea flux (2068 ± 1569 kmol s^{-1}) must be driven by the solubility pump (1625 ± 595 kmol s^{-1}) as the influence of the biological pump is small (110 ± 1458 kmol s^{-1}).

[64] The extended TIC^{π} budget shown in Figure 9b is to be compared with its initial picture in Figure 7c. The air to sea CO_2 flux in the Arctic-Subpolar region is considerably reduced form the initial 1131 ± 726 to 692 ± 600 kmol s^{-1}. Likewise, in the Temperate region the pre-industrial CO_2 air to sea flux is reduced from 1929 ± 701 to 1747 ± 717 kmol s^{-1}. Both reductions stem from the imbalance between

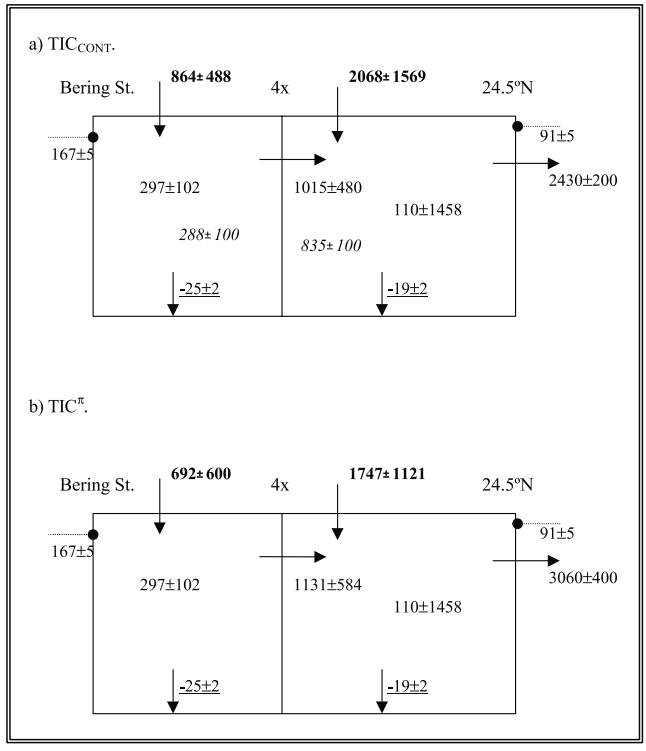

Figure 9. Schematic summary of the regional extended inorganic carbon budgets in the North Atlantic. These budgets take into account the transports across sections (plain numbers), the contribution of the river runoff (point-ended arrows and plain numbers), the carbonate sedimentation (arrows and underlined numbers), the net production (plain numbers) of inorganic carbon, a minus (plus) stands for consumption (production) of inorganic carbon within each defined box, and finally the storage of anthropogenic carbon (italic numbers). The air-sea fluxes are the calculated term (indicated by arrows and bold numbers). All the rates are in kmol s^{-1} (1 Gt C yr^{-1} = 2642 kmol s^{-1}). Budgets for (a) the contemporary total inorganic carbon (TIC_{CONT}) and (b) preindustrial total inorganic carbon (TIC^{π}). The Bering Strait contribution in the transports across sections has been ignored for consistency.

the riverine input, biological remineralization and calcite sedimentation all of which contribute to a net production of TIC in both regions. Our results point to the North Atlantic Ocean north of 24.5°N as a remarkable CO_2 sink of 2439 kmol s^{-1} during preindustrial times [*Holfort et al.*, 1998; *Keeling et al.*, 1989], slightly lower than the contemporary CO_2 sink of 2907 kmol s^{-1}.

[65] The combination of the contemporary, preindustrial and anthropogenic TIC budgets (Figures 9a, 9b, and Figure 7b, respectively) provides a composite and complete view of the inorganic carbon budget north of 24.5°N in the North Atlantic. We are aware that the differences between the initial and the extended budget results are dwarfed by the uncertainties, but it should be remembered that the uncertainties represent worst-case scenarios (see the Appendix). Despite this hindrance (not only in this work but also in similar ones), a consistent picture of the

role of the North Atlantic Ocean in the inorganic carbon cycle is emerging.

[66] According to our results the large TIC transport across 24.5°N is mainly driven by the air-sea CO_2 uptake north of 24.5°N, but only 17% of the air-sea flux corresponds to the anthropogenic signal. North of the 24.5°N the ocean is accumulating anthropogenic carbon at 1123 kmol s^{-1}, 44% directly taken up through the air-sea interface, and the remaining 56% is advected northward in the upper limb of the thermohaline circulation as also concluded by *Holfort et al.* [1998] and *Rosón et al.* [2002]. The C_{ANT} air-sea uptake is concentrated in the Temperate North Atlantic with a rate of 1.35 mmol m^{-2} d^{-1} compared to 0.90 mmol m^{-2} d^{-1} in the Arctic-Subpolar region. The mechanism explaining the lower C_{ANT} uptake in the northern region is the following, as proposed by *Wallace* [2001]: Warm waters flowing northward are practically pre-equilibrated with atmospheric CO_2 before sinking and returning to the south, therefore, little additional C_{ANT} would be taken up in the northern North Atlantic. According to this argument our results for the C_{ANT} air-sea flux are in agreement with the higher heat convergence or heat loss to the atmosphere in the Temperate region, 0.82 PW, relative to 0.65 PW north of the 4x section.

[67] Recently, *Orr et al.* [2001] estimated and compared the anthropogenic carbon uptake from four different 3-D global ocean models. Despite regional differences among models, the general trend in the North Atlantic shows that C_{ANT} air-sea uptake and accumulation mainly occurs in the Temperate region, in agreement with our findings. However, model results compared with data-based C_{ANT} inventories calculated by *Gruber et al.* [1996] in the North Atlantic are substantially lower. *Orr et al.* [2001] ascribed the differences to the poor skill of models to reproduce mixing and exchange between surface and deeper waters, through the processes of upwelling and convection, which ultimately control meridional transport.

[68] Our results directly contrast with the model-derived findings of *Sarmiento et al.* [1995] who attribute most of the current air-sea CO_2 flux in the North Atlantic to anthropogenic carbon, with even a small CO_2 outflux in the preindustrial era. As further discussed by *Murnane et al.* [1999] the Princeton Ocean Biogeochemical Model used by *Sarmiento et al.* [1995] underestimates the heat transport and consequently the Atlantic overturning circulation. Deficiencies in the underlying physical model, as also concluded by *Stephens et al.* [1998], would lead to underestimate the CO_2 transport in the ocean. If this is the case, CO_2 fluxes would be also underestimated. Despite this, the *Murnane et al.* [1999] and *Sarmiento et al.* [1995] estimates of CO_2 uptake between 18°S and 78°N in the Atlantic ocean agree with the data-based estimate given by *Takahashi et al.* [1995]. Furthermore, the recent paper by *Sarmiento et al.* [2000] compares the sea-air CO_2 flux and transport produced by three different Ocean Carbon Cycle Models, also confirming the agreement between the Princeton model output and the data-based interpolation by *Takahashi et al.* [1999], at least at a global scale. Therefore, we have two potential possibilities: either model-derived air-sea CO_2 fluxes [*Murnane et al.*, 1999; *Sarmiento et al.*, 1995, 2000] are as reliable as simple model interpolation schemes for the air-sea gradient and fluxes of CO_2 [*Takahashi et al.*, 1995, 1999]; or these two approximations for quantifying the air-sea CO_2 flux still present some deficiencies not yet accounted for but have compensating errors. A recent paper by *Doney* [1999] identified the tasks not yet resolved by ocean models to better understand the present ocean biogeochemistry and to predict future anthropogenic perturbations. The most important topics outlined were a better representation of the community structure, of the exchanges between open ocean, land, coastal ocean and atmosphere, and of the large-scale physical circulation along with mesoscale space and time variability. In the context of our budgets for inorganic carbon performed on a basin scale, we conclude that the main topics are better representation of the large-scale physical circulation in Global Circulation Models and better representation of the exchanges between open and coastal ocean, atmosphere and land in Global Biogeochemical Models.

6. Summary and Concluding Remarks

[69] The circulation pattern across the WOCE A25, 4x section was approximated by constraining the mass transport at specific areas and levels with literature-available transport values. Furthermore, an inverse model was set up to conserve the salt and mass transports across the section as we considered the North Atlantic Ocean to be a closed basin. Also, the silicate transport was constrained to its river input north of the section [*Tréguer et al.*, 1995].

[70] The chemical fields for TA, TIC and C_{ANT} were combined with the velocity field so as to obtain the net transport of these properties across the section. Both the chemical and velocity fields were decomposed into their barotropic, baroclinic and horizontal components with the aim of giving insights about the mechanisms leading to the transports. The main sources of uncertainty concerning the transports were evaluated, giving the maximum error in the estimates.

[71] The TA transport across the North Atlantic Subpolar gyre is practically negligible (-135 ± 507 kmol s^{-1}), in agreement with zero salt transport. TIC is transported SW at -1081 ± 490 kmol s^{-1}. However, as the section was sampled in summer, winter mixed layer values were simulated by homogenizing the upper 210 dbar with the TIC content at that pressure to determine a winter transport value of -949 kmol s^{-1}. Thus the mean annual transport of TIC is estimated to be -1015 ± 490 kmol s^{-1}.

[72] C_{ANT} was estimated using the back-calculation technique by *Gruber et al.* [1996] with the improvements suggested by *Pérez et al.* [2002]. The upper 130 dbar were homogenized in C_{ANT} in order to avoid an overestimate of C_{ANT} due to biological activity. C_{ANT} is advected northwards into the Subpolar gyre at a rate of 116 ± 125 kmol s^{-1}.

[73] The net mass transport across the section -0.4 ± 1.5 Sv accounts for the net precipitation plus runoff over evaporation north of the section. This transport drives a SW barotropic transport of salt that is balanced by the baroclinic plus horizontal components just as for the case of TA. For TIC, the SW barotropic transport is complemented by the baroclinic or overturning component giving rise to

the final SW transport value, as the horizontal transport is practically zero.

[74] The main mechanism explaining the net NE transport of C_{ANT} across the 4x section is the overturning circulation, which surpasses the SW barotropic and horizontal components. The overturning cell operates as a pump in which C_{ANT}-enriched waters flow NE above 1000 dbar, whereas relatively C_{ANT}-poor water flow SW at intermediate levels. The upper level directly advects C_{ANT} into the Subpolar gyre while the intermediate layer leaves C_{ANT}-enriched waters north of the section, acting indirectly as a pump of C_{ANT} towards the north.

[75] The large scale gyre or horizontal circulation has two major contributors, the North Atlantic Current and the East Greenland Current systems. They both horizontally remove TIC and C_{ANT} from the Subpolar North Atlantic north of the 4x section.

[76] Contemporary, preindustrial and anthropogenic TIC budgets were performed for the Arctic-Subpolar region north of the 4x section, and for the Temperate region, between the 4x and the 24.5°N sections, combining our results with those from *Rosón et al.* [2002] for 24.5°N. In a first approximation, contemporary TIC convergences/divergences were balanced by the air-sea exchange and the regional anthropogenic accumulation or C_{ANT} storage.

[77] In this work we have derived the regional C_{ANT} storage rates assuming that anthropogenic carbon is a conservative tracer that has reached its transient steady state. Consequently, the C_{ANT} storage can be calculated from the C_{ANT} Mean Penetration Depth (MPD) times the increase of C_{ANT} in the mixed layer. MPD values were calculated in the Subpolar and Temperate regions, distinguishing between the western and eastern basins. Publicly available CO_2 data from the OacesNAtlII-93 and WOCE A20 along with the 4x data were used for these calculations. A mean C_{ANT} increase rate in the upper mixed layer of 0.85 μmol kg^{-1} yr^{-1} was combined with the MPD data to estimate the rate of increase of C_{ANT} over time for each region.

[78] The inclusion of other terms (river input, biological production of TIC, sedimentation of calcium carbonate) has up to now been avoided except in a few instances due to lack of information about any of these topics on a regional scale. Here, we attempted extended budgets taking into account these terms. Biological net production of TIC (remineralization of organic matter from autotrophes and heterotrophes minus photosynthetic production within the whole water column) was indirectly derived from regional nitrate budgets. Inorganic carbon riverine input and calcium carbonate deposition were taken from the literature. While the results are tentative, they provide a framework for planning future basin-scale budgets.

[79] The contemporary TIC budget confirms the role of the North Atlantic Ocean north of 24.5°N as a strong atmospheric CO_2 sink, whose magnitude decreases from 3553 ± 991 kmol s^{-1} in the initial case to 2932 ± 2057 kmol s^{-1} when including additional terms in the extended budgets. Most of this flux occurs in the Temperate region, 63% initially and 71% in the extended case. Similar conclusions can be derived in the case of the preindustrial TIC budget, an initial sink of 3060 ± 1427 kmol s^{-1} compared to 2439 ± 1721 kmol s^{-1} in the extended case, distributed as in the contemporary budget.

[80] The C_{ANT} budget reveals the North Atlantic north of 24.5°N to be a store of anthropogenic carbon, which is accumulating at a rate of 1123 ± 200 kmol s^{-1}. Only 44% is directly taken up through the air-sea interface, most of the C_{ANT} is advected into the region in the upper limb of the overturning circulation. Contrary to expectations, this air-sea uptake of C_{ANT} mainly occurs in the Temperate region, not in the Arctic-Subpolar region where water masses are formed. The mechanism explaining this fact is simple, upwelling of old and C_{ANT} poor waters occurs in the equatorial area, in their transit northwards these waters cool and equilibrate with atmospheric CO_2, taking up atmospheric C_{ANT}. Therefore, when they arrive at deep-water formation areas they can take up little more C_{ANT}. Thus, C_{ANT} is taken up and transported northwards in the upper limb of the overturning circulation to be finally carried to depth in the northern end of the limb. Thus, C_{ANT} is transported southward in the Deep Western Boundary Current and is accumulating in the Temperate North Atlantic since no C_{ANT} flows southward across 24.5°N according to *Rosón et al.* [2002].

[81] Our results for contemporary air-sea CO_2 flux compare poorly with those from models and climatologies which are also based on a transport model. However, it should be taken into account that any of the fluxes still present remarkable uncertainty. In support of our results it is known that there remain major deficiencies in global carbon cycle models which are not yet resolved, especially those dealing with vertical mixing and overturning circulation, i.e., the underlying physical model. Also, the models do not consider simultaneously the heat, nutrient and carbon budgets as we have tried to do here.

[82] Transport estimates for TIC and C_{ANT} provide valuable independent information about the regional distribution of air-sea CO_2 uptake, both for the natural and the anthropogenic signals. In particular, the natural and anthropogenic carbon fluxes are potential constraints or tests for global carbon models and can be used to improve their skill to reproduce and eventually predict the oceanic anthropogenic carbon uptake.

Appendix A: Uncertainties in the Transports

[83] In this section we discuss the main sources of error affecting the transport estimates, evaluating the same factors as given by *Álvarez et al.* [2002]. These are: the precision of the measurements, their temporal variability, the spatial resolution of the sampling and errors due to the specification of the Ekman layer transport, the sensitivity of our calculations to the imposed circulation on certain areas (the CGFZ, the EGC and the IAP), as well as the silicate constraint. We evaluated the worst situation and considered the sources as independent and uncorrelated, thus the final error estimates stand for maximum uncertainties in the final transport values.

A1. Measurements Errors

[84] Errors due to the uncertainty in pressure, salinity and temperature determination have a negligible effect on the

Table A1. "Best Estimate" Final Transports Across the 4x Section and Flux Errors Due to Uncertainties in the Measurements or Methodology (*Meas.*), the Eddy Resolution (*Eddy*), Variations in the Ekman Transport (*Ekman*), the Patterns of Circulation Across the Section (*Circ.*), The Inverse Model (*Inv.*), the Silicate Constraint (*Silicate*) and Bottom Triangles (*BT*)[a]

	Final	Meas.	Eddy	Ekman	Circ.	Inv.	Silicate	BT	Total
Mass -Sv	−0.40	0	1.25	0.14	0.02	0.04	0.01	0.02	1.48
Salt - Mkg s^{-1}	−0.8	0	0.5	4.9	0.7	0.2	0.1	0.3	6.7
TA - kmol s^{-1}	−135	4	25	329	34	96	17	2	507
TIC - kmol s^{-1}	−1081	8	10	297	58	97	10	10	490
C_{ANT} - kmol s^{-1}	116	21	4	7	22	39	12	20	125

[a]Units are Sv (10^6 m3 s^{-1}), Mkg s^{-1} (10^6 kg s^{-1}) and kmol s^{-1} (10^3 mol s^{-1}).

mass transport [*Holfort and Siedler*, 2001]. Chemical properties, TA, TIC and C_{ANT}, have a maximum error of ±2, ±3 and ±8 μmol kg^{-1}, respectively. About thirty normally distributed random perturbations of the corresponding order of magnitude were introduced in the TA, TIC and C_{ANT} fields along the section. The range of variability of the new transports was 4, 8 and 21 kmol s^{-1}, for TA, TIC and C_{ANT}, respectively, thus revealing that the measurement uncertainty makes a relatively small contribution to the total error (See Table A1).

A2. Temporal Variability Errors

[85] As also explained by *Álvarez et al.* [2002], we are assuming our section to be representative of a climatological mean. Thus, we are implicitly ignoring any decadal or interannual changes in the thermohaline or chemical characteristics of the water masses. Seasonal variability is more pronounced in the Ekman layer and will be mentioned in the paragraph dealing with errors due to this component.

A3. Spatial Resolution Error

[86] As explained by *Álvarez et al.* [2002], the 4x stations are close enough to resolve the main eddy scale. On the other hand, the effect of reducing the spatial resolution was assessed by reducing by a half the number of stations and constraining again the velocity field. In this way, the TA, TIC and C_{ANT} transports change to 110, −1013 and 44 kmol s^{-1}. The most notable reduction occurs in the C_{ANT} transport, pointing to the importance of resolving the horizontal scale when designing a section, as also concluded by *Rosón et al.* [2002] when comparing their results from the 24.5°N North Atlantic section with those from *Brewer et al.* [1989] along the same latitude but with a very reduced spatial coverage.

[87] It is possible to make some estimate of the error incurred due to eddy activity by considering that the transport of each property has an error equal to the standard deviation (STD) of the eddy transport between station pairs. This STD is modified by a normally distributed random number, this modification is done about a hundred times to reflect the number of stations, and the STD of the net eddy flux for the complete section is calculated. We evaluate the error due to eddy activity as equal to this final STD. See Table A1 for the estimated eddy error contribution of each property to the total flux error.

A4. Ekman Error

[88] Uncertainties in the Ekman transport arise from differences in wind stress climatologies, the Ekman layer depth and the seasonal variability of the wind stress and chemical concentrations in the upper layer. *Holfort et al.* [1998] determined that the main source of uncertainty in the Ekman layer transport arises from uncertainties in the wind stress data. We have calculated the annual mean wind stress from mean and seasonal wind stress values obtained from the SOC climatology which is considered suitable for the WOCE sampling period [*Josey et al.*, 2002]. The uncertainty in the transports was simulated allowing a variation of ±10% in the strength of the Ekman mass flux. See Table A1.

A5. Circulation Error

[89] The sensitivity of the fluxes to changes in the circulation was assessed by varying our imposed mass transports in the CGFZ, the EGC and the IAP according to data in the literature. The circulation errors were calculated as half of the range of the new transports (Table A1) and mainly arise from alterations in the strength of the EGC. See *Álvarez et al.* [2002] for a more detailed explanation.

A6. Inversion Error

[90] The imposed constraints (mass and salt conservation, a silicate flux equal to −26 kmol s^{-1}, mass transports over the CGFZ, IAP and east of Greenland according to the bibliography) have as well a range of uncertainty, affecting the mass and therefore, the chemical transports. Their evaluation is explained elsewhere [*Álvarez et al.*, 2002] and, the results are given in Table A1. Within the inverse model error, we must consider that related to the silicate constraint. Its relevance is assessed allowing a variation of ±15% around the −26 kmol s^{-1} value.

A7. Bottom Triangle Error

[91] The velocity and property distribution in the Bottom Triangle (BT) can be approximated in different ways: some authors do not consider the flow across the BT when the velocity field has been already designed to conserve mass [e.g., *Lavín et al.*, 1998]; others assume that the velocity decreases linearly from the deepest common level to the bottom [e.g., *Holfort and Siedler*, 2001].

[92] In this work the velocity in the BT is approximated to be the same as the velocity at the deepest common level of each pair of stations. Correspondingly, the BT properties are calculated as a weighted-mean taking into account the number of 20 dbar layers below the maximum common level:

$$\mathrm{PropMean} = \frac{\sum_1^{nn} \mathrm{Prop}(MCL + ii)^*(nn + 1 - ii)}{nn^*(nn + 1)/2}$$

where PropMean is the weighted mean of the property at the BT, MCL is the Maximum Common Level, Prop is the property concentration below the MCL at the deepest station within each pair, *nn* is the number of levels below the MCL. Thus, the average property in the bottom triangle is a triangle-weighted average of the property profile at the deeper station and we consider this estimate to have a negligible error for the BT property. Since the BT transport should only be smaller than the approximation considered here, we recalculated the circulation field in the same way but assuming no transport in the BT. The difference between the two approximations is taken here as the error due to the BT definition (Table A1). The small error due to BT variations is a result of the fact that with and without BT transport the circulation pattern is constrained similarly and that the section-averaged property is not very different from the BT property for most of the properties. Note, however, that the BT error ascribed to C_{ANT} is slightly higher, due to the fact that BT C_{ANT} values are much lower than the section mean.

[93] In this analysis, we have tried to assess the main sources of uncertainty in the estimated transports across the 4x section, obtaining their maximum values. Uncertainties in the Ekman mass transport mainly affect the salt transport which should be conserved across the section, having a direct impact on the TA and TIC transports due to their specific relationship with salinity (about 67 and 60 μmol kg^{-1} $salinity^{-1}$, respectively). Uncertainties in the C_{ANT} transport are mainly ascribed to the uncertainty in the mass transport across the section (circulation, inversion and silicate errors) with a relatively high contribution ascribed to the uncertainty in the back-calculation technique used to estimate C_{ANT}. The BT C_{ANT} definition has, as well, a relatively high impact on the final error ascribed to the C_{ANT} transport.

A8. Error Estimation on the Budgets

[94] The budgets of dissolved inorganic carbon and nitrate performed in this work assume steady state for the variables on timescales of the order of the flushing time of the region considered. A maximum error is assigned to every known term of the balance (e.g., fluxes across sections, denitrification, atmospheric inputs, sedimentation, etc.). In the case of the transports across the sections, the error is taken from the literature or directly from our estimates. A normally distributed random number multiplies these maximum errors, the calculated number is then added to the initial values. Next, the inferred quantity is calculated. This procedure is repeated a hundred times. Finally the standard deviation of the resulting set of fluxes is obtained. This STD corresponds to the error on the inferred variable in the budget equation.

[95] **Acknowledgments.** We are grateful to Sheldon Bacon, Principal Scientist, the Captain, officers and crew of the RRS *Discovery* and to the science team for their hard work during the 4x cruise. The cruise was primarily supported by the Natural Environment Research Council (NERC) under the UK WOCE Community Research Programme. Our special thanks to Iris Soler Arístegui for her valuable help and support with the analysis and sampling during the cruise. The Spanish participation in the 4x cruise was funded by the Spanish CICYT project MAR-97-1622-E. The stay of M. Álvarez at SOC was financed by a "Beca de estancia no estranxeiro" and a "Beca Predoutoral" from the Xunta de Galicia. M. Álvarez was also financed by CAVASSOO (EVK2-CT-2000-00088). The authors would like to thank the valuable suggestions and comments of X.A. Álvarez-Salgado and D.W. Wallace. This work would not have been possible without the effort of the scientific staff, officers and crew of the OACES program in the North Atlantic carried by the NOAA Atlantic Oceanographic and Meteorological Laboratory (AOML) and the Pacific Marine Environmental Laboratory (PMEL), and those involved in the WOCE A20 cruise carried by the Woods Hole Oceanographic Institution (WHOI). Our special thanks to the Oak Ridge Carbon Dioxide Information Analysis Center (CDIAC) for providing high-quality CO_2 data sets to the research community. We also thank two anonymous reviewers for their helpful suggestions.

References

Altabet, M. A., Particulate net nitrogen fluxes in the Sargasso Sea, *J. Geophys. Res.*, *94*, 12,771–12,780, 1989.

Álvarez, M., H. L. Bryden, F. F. Pérez, A. F. Ríos, and G. Rosón, Physical and biogeochemical fluxes and net budgets in the Subpolar and Temperate North Atlantic, *J. Mar. Res.*, *60*, 191–262, 2002.

Anderson, L. A., and J. L. Sarmiento, Redfield ratios of remineralization determined by nutrient data analysis, *Global Biogeochem. Cycles*, *8*, 65–80, 1994.

Anderson, L. G., K. Olsson, E. P. Jones, M. Chierici, and A. Fransson, Anthropogenic carbon dioxide in the Arctic Ocean: Inventory and sinks, *J. Geophys. Res.*, *103*, 27,707–27,716, 1998a.

Anderson, L. G., K. Olsson, and M. Chierici, A carbon budget for the Arctic Ocean, *Global Biogeochem. Cycles*, *12*, 455–465, 1998b.

Anderson, L. G., M. Chierici, and E. Fogelqvist, Flux of anthropogenic carbon into the deep Greenland Sea, *J. Geophys. Res.*, *105*, 14,339–14,345, 2000.

Aumont, O., J. C. Orr, P. Monfray, W. Ludwig, P. Amiotte-Suchet, and J. L. Probst, Riverine-driven interhemispheric transport of carbon, *Global Biogeochem. Cycles*, *15*, 393–405, 2001.

Bacon, S., Circulation and fluxes in the North Atlantic between Greenland and Ireland, *J. Phys. Oceanogr.*, *27*, 1420–1435, 1997.

Bacon, S., RRS *Discovery* cruise 230, 07-Aug-17 Sep 1997: Two hydrographic sections across the boundaries of the Subpolar Gyre: FOUREX, *Cruise Rep. 16*, 104 pp., Southampton Oceanogr. Cent., Southampton, England, 1998.

Bates, N. R., A. F. Michaels, and A. H. Knap, Seasonal and interannual variability of oceanic carbon dioxide species at the U.S. JGOFS Bermuda Atlantic Time-series Study (BATS) site, *Deep Sea Res., Part II*, *43*, 347–383, 1996.

Baumgartner, A., and E. Reichel, *The World Water Balance*, 179 pp., Elsevier Sci., New York, 1975.

Berner, E. K., and R. A. Berner, *The Global Water Cycle*, 397 pp., Prentice-Hall, Old Tappan, N. J., 1987.

Brewer, P., Direct observation of the oceanic CO_2 increase, *Geophys. Res. Lett.*, *5*, 997–1000, 1978.

Brewer, P., C. Goyet, and D. Dyrssen, Carbon dioxide transport by ocean currents at 25°N latitude in the Atlantic Ocean, *Science*, *246*, 477–479, 1989.

Broecker, W. S., and T. H. Peng, *Tracers in the Sea*, 690 pp., Lamont-Doherty Earth Observ., Palisades, N. Y., 1982.

Broecker, W. S., and T. H. Peng, Interhemispheric transport of carbon dioxide by ocean circulation, *Nature*, *356*, 587–589, 1992.

Broecker, W. S., and T. H. Peng, Evaluation of the ^{13}C constraint on the uptake of fossil-fuel CO_2 by the ocean, *Global Biogeochem. Cycles*, *7*, 619–626, 1993.

Broecker, W. S., T. Takahashi, H. J. Simpson, and T. H. Peng, Fate of fossil fuel carbon dioxide and the global carbon budget, *Science*, *206*, 409, 1979.

Bryden, H. L., Ocean heat transport across 24° latitude, in *Interactions Between Global Climate Subsystems: The Legacy of Hann*, *Geophys. Monogr. Ser.*, vol. 75, edited by G. A. McBean and M. Hantel, pp. 65–75, AGU, Washington, D. C., 1993.

Bryden, H. L., D. H. Roemmich, and J. A. Church, Ocean heat transport across 24°N in the Pacific, *Deep Sea Res.*, *38*, 297–324, 1991.

Chen, C.-T. A., and F. Millero, Gradual increase of oceanic CO_2, *Nature*, *277*, 205–206, 1979.

Clayton, T., and R. H. Byrne, Spectrophotometric seawater pH measurements: Total hydrogen ion concentration scale calibration of m-cresol purple and at-sea results, *Deep Sea Res., Part I*, *40*, 2115–2129, 1993.

Culberson, C. H., WOCE Operations Manual (WHP Operations and Methods), *WHPO 91/1*, 15 pp., WOCE Hydrogr. Program Off., La Jolla, Calif., 1991.

Cunningham, S. A., and T. W. N. Haine, Labrador Sea water in the eastern North Atlantic, I, A synoptic circulation inferred form a minimum in potential vorticity, *J. Phys. Oceanogr.*, *25*, 649–665, 1995.

Dickson, A. G., An exact definition of total alkalinity and procedure for the estimation of alkalinity and total inorganic carbon from titration data, *Deep Sea Res.*, *28*, 609–623, 1981.

Doney, S. C., Major challenges confronting marine biogeochemistry modelling, *Global Biogeochem. Cycles*, *13*, 705–714, 1999.

Doney, S. C., D. W. R. Wallace, and H. W. Ducklow, The North Atlantic carbon cycle: New perspectives from JGOFS and WOCE, in *The Changing Ocean Carbon Cycle*, edited by R. B. Hanson, H. W. Ducklow, and J. G. Field, Cambridge Univ. Press, New York, 2000.

Drever, J. L., Y.-H. Li, and J. B. Maynard, *Chemical Cycles in the Evolution of the Earth*, edited by C. G. Gregor et al., pp. 17–53, John Wiley, New York, 1988.

Gammon, R. H., J. Cline, and D. Wisegarver, Chlorofluoromethanes in the northeast Pacific Ocean: Measured vertical distributions and application as transient tracers of upper ocean mixing, *J. Geophys. Res.*, *87*, 9441–9454, 1982.

Gruber, N., Anthropogenic CO_2 in the Atlantic Ocean, *Global Biogeochem. Cycles*, *12*, 165–191, 1998.

Gruber, N., J. L. Sarmiento, and T. F. Stocker, An improved method for detecting anthropogenic CO_2 in the oceans, *Global Biogeochem. Cycles*, *10*, 809–837, 1996.

Holfort, J., and G. Siedler, The meridional oceanic transports of heat and nutrients in the South Atlantic, *J. Phys. Oceanogr.*, *31*, 5–29, 2001.

Holfort, J., K. M. Johnson, B. Scheider, G. Siedler, and D. W. R. Wallace, Meridional transport of dissolved inorganic carbon in the South Atlantic Ocean, *Global Biogeochem. Cycles*, *12*, 479–499, 1998.

Hoppema, M., E. Fahrbach, M. H. C. Stoll, and H. J. W. de Baar, Increase of carbon dioxide in the bottom water of the Weddell Sea, Antarctica, *Mar. Chem.*, *59*, 201–210, 1998.

Howarth, R. W., et al., Regional nitrogen budgets and riverine N & P fluxes for the drainages to the North Atlantic Ocean: Natural and human influences, *Biogeochemistry*, *35*, 75–139, 1996.

Jenkins, W. J., Nitrate flux into the euphotic zone near Bermuda, *Nature*, *331*, 521–523, 1988.

Jenkins, W. J., and J. C. Goldman, Seasonal cycling and primary production in the Sargasso Sea, *J. Mar. Res.*, *43*, 465–491, 1985.

Joos, F., J. L. Sarmiento, and U. Siegenthaler, Estimates of the effect of Southern Ocean iron fertilization on atmospheric CO_2 concentrations, *Nature*, *349*, 772–775, 1991a.

Joos, F., U. Siegenthaler, and J. L. Sarmiento, Possible effects of iron fertilization in the Southern Ocean on atmospheric CO_2 concentration, *Global Biogeochem. Cycles*, *5*, 135–150, 1991b.

Josey, S. A., E. C. Kent, and P. K. Taylor, On the wind stress forcing of the ocean in the SOC climatology: Comparisons with the NCEP/NCAR, ECMWF, UWM/COADS and Hellerman and Rosenstein datasets, *J. Phys. Oceanogr.*, *32*, 1993–2019, 2002.

Keeling, C. D., S. C. Piper, and M. Heiman, A three-dimensional model of atmospheric CO_2 transport based on observed winds: Four mean annual gradients and interannual variations, in *Aspects of Climate Variability in the Pacific and Western Americas*, *Geophys. Monogr. Ser.*, vol. 55, edited by D. H. Peterson, pp. 305–363, AGU, Washington, D. C., 1989.

Keeling, C. D., S. C. Piper, and M. Heiman, Global and hemispheric CO_2 sinks deduced from changes in atmospheric O_2 concentration, *Nature*, *381*, 218–221, 1996.

Keeling, R. F., and T.-H. Peng, Transport of heat, CO_2 and O_2 by the Atlantic's thermohaline circulation, *Philos. Trans. R. Soc. London, Ser. B*, *348*, 133–142, 1995.

Keeling, R. F., and S. R. Shertz, Seasonal and interannual variations in the atmospheric oxygen and implications for the global carbon cycle, *Nature*, *358*, 723–727, 1992.

Keeling, R. F., R. P. Najjar, M. L. Bender, and P. P. Tans, What atmospheric oxygen measurements can tell us about the global carbon cycle, *Global Biogeochem. Cycles*, *7*, 37–67, 1993.

Körtzinger, A., L. Mintrop, and J. C. Duinker, On the penetration of anthropogenic CO_2 into the North Atlantic Ocean, *J. Geophys. Res.*, *103*, 18,681–18,689, 1998.

Lavín, A., Fluxes, trends and decadal changes in the subtropical North Atlantic, Ph.D thesis, Univ. of Santander, Santander, Spain, 1999.

Lavín, A., H. L. Bryden, and G. Parrilla, Meridional transport and heat flux variations in the subtropical North Atlantic, *Global Atmos. Ocean Syst.*, *6*, 269–293, 1998.

Lipschultz, F., and N. J. P. Owens, An assessment of nitrogen fixation as a source of nitrogen to the North Atlantic, *Biogeochemistry*, *35*, 261–274, 1996.

Lundberg, L., and P. M. Haugan, A Nordic Seas-Arctic Ocean carbon budget from volume flows and inorganic carbon data, *Global Biogeochem. Cycles*, *10*, 493–510, 1996.

Martel, F., and C. Wunsch, The North Atlantic circulation in the early 1980s: An estimate from inversion of a finite difference model, *J. Phys. Oceanogr.*, *29*, 283–383, 1993.

Mehrbach, C., C. H. Culberson, J. E. Hawley, and R. M. Pytkowicz, Measurements of the apparent dissociation constant of carbonic acid in seawater at atmospheric pressure, *Limnol. Oceangr.*, *8*, 897–907, 1973.

Meybeck, M., Global chemical weathering of surficial rocks estimated from river dissolved load, *Am. J. Sci.*, *287*, 401–428, 1987.

Milliman, J. D., Production and accumulation of calcium carbonate in the ocean: Budget of a non steady state, *Global Biogeochem. Cycles*, *7*, 927–957, 1993.

Murnane, R. J., J. L. Sarmiento, and C. Le Quéré, Spatial distribution of air-sea CO_2 fluxes and the interhemispheric transport of carbon by the oceans, *Global Biogeochem. Cycles*, *13*, 287–305, 1999.

Neftel, A., H. Friedli, E. Moor, H. Lötscher, H. Oeschger, U. Siegenthaler, and B. Stauffer, Historical CO_2 record from the Siple station ice core, in *Trends '93: A compendium of Data on Global Change*, edited by T. Boden et al., *Rep. ORNL/CDIAC-65,* pp. 11–14, Carbon Dioxide Inf. Anal. Cent., Oak Ridge Natl. Lab., Oak Ridge, Tenn., 1994.

Nixon, S. W., et al., The fate of nitrogen and phosphorus at the land-sea margin of the North Atlantic Ocean, *Biogeochemistry*, *35*, 141–180, 1996.

Orr, J. C., Accord between ocean models predicting uptake of anthropogenic CO_2, *Water Air Soil Pollut.*, *70*, 465–481, 1993.

Orr, J. C., et al., Estimates of anthropogenic carbon uptake from four three-dimensional global ocean models, *Global Biogeochem. Cycles*, *15*, 43–60, 2001.

Pérez, F. F., and F. Fraga, A precise and rapid analytical procedure for alkalinity determination, *Mar. Chem.*, *21*, 169–182, 1987.

Pérez, F. F., M. Álvarez, and A. F. Ríos, Improvements on the back-calculation technique for estimating anthropogenic CO_2, *Deep Sea Res., Part I*, *49*, 859–875, 2002.

Prospero, J. M., K. Barrett, T. Church, F. Dentener, R. A. Duce, J. N. Galloway, H. Levy II, J. Moody, and P. Quinn, Atmospheric deposition of nutrients to the North Atlantic Basin, *Biogeochemistry*, *35*, 27–73, 1996.

Quay, P. D., B. Tillbrook, and C. S. Wong, Oceanic uptake of fossil fuel CO_2: Carbon-13 evidence, *Science*, *256*, 74–79, 1992.

Rintoul, S. R., and C. Wunsch, Mass, heat, oxygen and nutrient fluxes and budgets in the North Atlantic Ocean, *Deep Sea Res.*, *38*, 355–377, 1991.

Ríos, A. F., F. F. Pérez, and F. Fraga, Long-term (1977–1997) measurements of CO_2 in the eastern North Atlantic: Evaluation of anthropogenic input, *Deep Sea Res., Part II*, *48*, 2227–2239, 2001.

Roach, A. T., K. Aagaard, C. H. Pease, S. A. Salo, T. Weingartner, V. Pavlov, and M. Kulakov, Direct measurements of transport and water properties through the Bering Strait, *J. Geophys. Res.*, *100*, 18,443–18,457, 1995.

Robbins, P. E., Direct observations of the meridional transport of total inorganic carbon in the south Atlantic Ocean (abstract), *EOS Trans. AGU*, *75*, Ocean Sci. Meet. Suppl., 161, 1994.

Roemmich, D., and C. Wunsch, Two transatlantic sections: Meridional circulation and heat flux in the subtropical North Atlantic Ocean, *Deep Sea Res.*, *32*, 619–664, 1985.

Rosón, G., A. F. Ríos, A. Lavín, F. F. Pérez, and H. L. Bryden, Carbon distribution, fluxes and budgets in the Subtropical North Atlantic Ocean (24.5°N), *J. Geophys. Res.*, doi:10.1029/1999JC000047, in press, 2002.

Sabine, C. L., R. M. Key, K. M. Johnson, F. J. Millero, A. Poisson, J. L. Sarmiento, D. W. R. Wallace, and C. D. Winn, Anthropogenic CO_2 inventory of the Indian Ocean, *Global Biogeochem. Cycles*, *13*, 179–198, 1999.

Sarmiento, J. L., and E. T. Sundquist, Revised budget for the oceanic uptake of anthropogenic carbon dioxide, *Nature*, *356*, 589–593, 1992.

Sarmiento, J. L., T. Herbert, and J. R. Toggweiler, Mediterranean nutrient balance and episodes of anoxia, *Global Biogeochem. Cycles*, *2*, 427–444, 1988.

Sarmiento, J. L., G. Thiele, R. M. Key, and W. S. Moore, Oxygen and nitrate new production and remineralization in the North Atlantic Subtropical Gyre, *J. Geophys. Res.*, *95*, 18,303–18,315, 1990.

Sarmiento, J. L., J. C. Orr, and U. Siegenthaler, A perturbation simulation of CO_2 uptake in an ocean general circulation model, *J. Geophys. Res.*, *97*, 3621–3645, 1992.

Sarmiento, J. L., R. Murnane, and C. Le Quere, Air-sea CO_2 transfer and the carbon budget of the North Atlantic, *Philos. Trans. R. Soc. London, Ser. B*, *348*, 211–219, 1995.

Sarmiento, J. L., P. Monfray, E. Maier-Reimer, O. Aumont, R. J. Murnane, and J. C. Orr, Sea-air CO_2 fluxes and carbon transport: A comparison of

three ocean general circulation models, *Global Biogeochem. Cycles*, *14*, 1267–1281, 2000.

Saunders, P. M., Circulation in the eastern North Atlantic, *J. Mar. Res.*, *40*, 641–657, 1982.

Saunders, P., The flux of overflow water through the Charlie-Gibbs Fracture Zone, *J. Geophys. Res.*, *99*, 12,343–12,355, 1994.

Saunders, P., and S. R. Thompson, Transport, heat, and freshwater fluxes within a diagnostic numerical model (FRAM), *J. Phys. Oceanogr.*, *23*, 452–464, 1993.

Schimel, D., et al., CO_2 and the carbon cycle, in *Climate Change 1995: The Science of Climate Change: Contribution of WG I to the Second Assessment Report of the IPCC*, edited by J. T. Houghton et al., pp. 65–83, Cambridge Univ. Press, New York, 1996.

Schindler, D. W., The mysterious missing sink, *Nature*, *398*, 105–107, 1999.

Schmitz, W. J., Jr., On the world ocean circulation, vol. I, Some global features/North Atlantic Circulation, *Tech. Rep. WHOI-96-03*, Woods Hole Oceanogr. Inst., Woods Hole, Mass., 1996.

Siegenthaler, U., and F. Joos, Use of a simple model for studying oceanic tracer distributions and the global carbon cycle, *Tellus, Ser. B*, *44*, 186–207, 1992.

Siegenthaler, U., and J. L. Sarmiento, Atmospheric carbon dioxide and the ocean, *Nature*, *365*, 119–125, 1993.

Stephens, B. B., R. F. Keeling, M. Heimann, K. D. Six, R. Murnane, and K. Caldeira, Testing global ocean carbon cycle models using measurements of atmospheric O_2 and CO_2 concentration, *Global Biogeochem. Cycles*, *12*, 213–230, 1998.

Stocker, T. F., W. S. Broecker, and D. G. Wright, Carbon uptake experiments with a zonally-averaged ocean circulation model, *Tellus, Ser. B*, *46*, 103–122, 1994.

Stoll, M. H. C., H. M. van Aken, H. J. W. de Baar, and C. J. de Boer, Meridional carbon dioxide transport in the northern North Atlantic, *Mar. Chem.*, *55*, 205–216, 1996.

Takahashi, T., T. T. Takahashi, and S. C. Sutherland, An assessment of the role of the North Atlantic as a CO_2 sink, *Philos. Trans. R. Soc. London, Ser. B*, *348*, 143–152, 1995.

Takahashi, T., R. H. Wanninkhof, R. A. Feely, R. F. Weiss, D. W. Chipman, N. Bates, J. Olafsson, C. Sabine, and S. C. Sutherland, Net sea-air CO_2 flux over the global oceans: An improved estimate based on the sea-air pCO_2 difference, in Proceedings of the 2nd International Symposium on CO_2 in the Oceans, *CGER-I037-'99*, pp. 9–15, Cent. For Global Environ. Res., Natl. Inst. for Environ. Stud., Tsukuba, Japan, 1999.

Tans, P. P., I. Y. Fung, and T. Takahashi, Observational constraints on the global atmospheric CO_2 budget, *Science*, *247*, 1431–1438, 1990.

Tans, P. P., J. A. Berry, and R. F. Keeling, Oceanic $^{13}C/^{12}C$ observations: A new window on ocean CO_2 uptake, *Global Biogeochem. Cycles*, *7*, 353–368, 1993.

Tréguer, P., D. M. Nelson, A. J. van Bennekom, D. J. DeMaster, A. Laynaert, and B. Quéguiner, The silicate balance in the world ocean: A reestimate, *Science*, *268*, 375–379, 1995.

U.N. Educational, Scientific, and Cultural Organization, Progress on oceanographic tables and standards 1983–1986: Work and recommendations of the UNESCO/SCOR/ICES/IAPSO Joint Panel, *UNESCO Tech. Pap. Mar. Sci.*, *50*, 1986.

Wallace, D. W. R., Monitoring global ocean inventories, *OOSDP Background Rep. 5*, 55 pp., Ocean Obs. Syst. Dev. Panel, Texas A&M Univ., College Station, Tex., 1995.

Wallace, D. W. R., Storage and transport of excess CO_2 in the Oceans: The JGOFS/WOCE Global CO_2 Survey. in *Ocean Circulation and Climate, Int. Geophys. Ser.*, vol. 77, edited by G. Siedler, J. Church, and J. Gould, pp. 489–520, Academic, San Diego, Calif., 2001.

Walsh, J. J., K. L. Carder, and F. E. Müller-Karger, Meridional flues of dissolved organic matter in the North Atlantic Ocean, *J. Geophys. Res.*, *97*, 15,625–15,637, 1992.

Wanninkhof, R., Relationship between wind speed and gas exchange over the ocean, *J. Geophys. Res.*, *97*, 7373–7383, 1992.

Wanninkhof, R., S. C. Doney, T. H. Peng, J. L. Bullister, K. Lee, and R. A. Feely, Comparison of methods to determine the anthropogenic CO_2 invasion into the Atlantic Ocean, *Tellus, Ser. B*, *51*, 511–530, 1999.

Watson, A. J., P. D. Nightingale, and D. J. Cooper, Modelling atmosphere-ocean CO_2 transfer, *Philos. Trans. R. Soc. London, Ser. B*, *348*, 125–132, 1995.

Weiss, R. F., Carbon dioxide in water and seawater: The solubility of a non ideal gas, *Mar. Chem.*, *2*, 203–215, 1974.

Wollast, R., Interactions of carbon and nitrogen cycles in the coastal zone, in *Interactions of C, N, P, and S Biogeochemical Cycles and Global Change, NATO ASI Ser.*, vol. 14, edited by R. Wollast, F. T. Mackenzie, and L. Chou, North Atlantic Treaty Org., Brussels, 1993.

M. Álvarez, F. F. Pérez, and A. F. Ríos, Instituto de Investigaciones Marinas (CSIC), Apartado 2026, 36208 Vigo, Spain. (malvarez@iim.csic.es; fizfperez@iim.csic.es; aida@iim.csic.es)

H. L. Bryden, Southampton Oceanography Centre, Empress Dock, Southampton, SO14 3ZH, UK. (hlb@soc.soton.ac.uk)

G. Rosón, Facultad de Ciencias, Universidade de Vigo, Campus Lagoas-Marcosende, 36200 Vigo, Spain. (groson@uvigo.es)

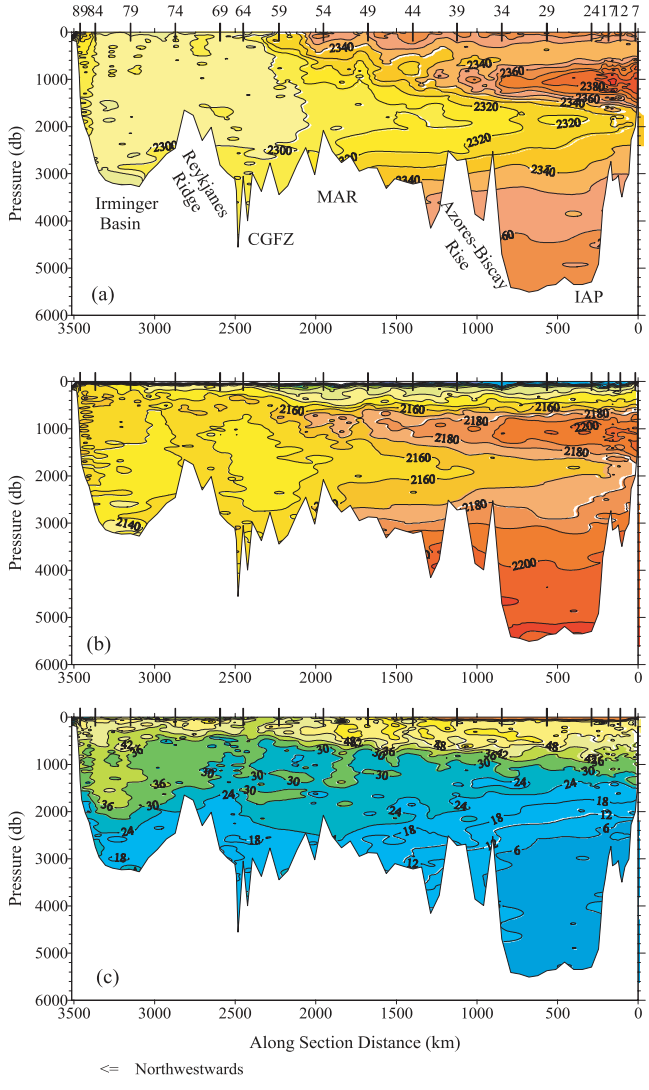

Figure 2. Vertical distribution along the 4x section of (a) total alkalinity (TA), (b) total inorganic carbon (TIC) and (c) anthropogenic carbon (C_{ANT}), all properties in μmol kg^{-1}. The upper axis shows station positions. Geographic areas are highlighted: MAR stands for Mid-Atlantic Ridge, CGFZ for Charlie-Gibbs Fracture Zone and IAP for Iberian Abyssal Plain.